The Astronomical Journal, 136:461–478, 2008 July doi:10.1088/0004-6256/136/1/461

STRUCTURAL PROPERTIES OF ULTRA-COMPACT DWARF GALAXIES IN THE FORNAX AND VIRGO CLUSTERS

E. A. Evstigneeva[1], M. J. Drinkwater[1], C. Y. Peng[2], M. Hilker[3], R. De Propris[4], J. B. Jones[5], S. Phillipps[6], M. D. Gregg[7,8], and A. M. Karick[7,8]

[1] Department of Physics, University of Queensland, QLD 4072, Australia; e.evstigneeva@gmail.com, m.drinkwater@uq.edu.au
[2] NRC Herzberg Institute of Astrophysics, 5071 West Saanich Road, Victoria, BC, V9E 2E7, Canada; cyp@nrc-cnrc.gc.ca
[3] European Southern Observatory, Karl-Schwarzschild-Str. 2, 85748 Garching bei München, Germany; mhilker@eso.org
[4] Cerro Tololo Inter-American Observatory, Casilla 603, La Serena, Chile; rdepropris@ctio.noao.edu
[5] Astronomy Unit, School of Mathematical Sciences, Queen Mary University of London, Mile End Road, London E1 4NS, UK; bryn.jones@qmul.ac.uk
[6] Astrophysics Group, Department of Physics, University of Bristol, Tyndall Avenue, Bristol BS8 1TL, UK; S.Phillipps@bristol.ac.uk
[7] Department of Physics, University of California, Davis, CA 95616, USA; gregg@igpp.ucllnl.org, akarick@igpp.ucllnl.org
[8] Institute for Geophysics and Planetary Physics, Lawrence Livermore National Laboratory, L-413, Livermore, CA 94550, USA

Received 2007 November 7; accepted 2008 April 21; published 2008 June 13

ABSTRACT

We present a detailed analysis of high-resolution two-band *Hubble Space Telescope* Advanced Camera for Surveys imaging of 21 ultra-compact dwarf (UCD) galaxies in the Virgo and Fornax Clusters. The aim of this work is to test two formation hypotheses for UCDs—whether they are bright globular clusters (GCs) or stripped ("threshed") early-type dwarf galaxies—by direct comparison of UCD structural parameters and colors with GCs and galaxy nuclei. We find that the UCD surface brightness profiles can be described by a range of models and that the luminous UCDs in particular cannot be described by standard King models with tidal cutoffs as they have extended outer halos. This is not expected from traditional King models of GCs, but is consistent with recent results for massive GCs. The total luminosities, colors, and sizes of the UCDs (their position in the color–magnitude and luminosity–size diagrams) are consistent with them being either luminous GCs or threshed nuclei of both early-type and late-type galaxies (not just early-type dwarfs). For the most luminous UCDs we estimate color gradients over a limited range of radius. These are systematically positive in the sense of getting redder outward: mean $\Delta(F606W - F814W) = 0.14$ mag per 100 pc with rms $= 0.06$ mag per 100 pc. The positive gradients found in the bright UCDs are consistent with them being either bright GCs or threshed early-type dwarf galaxies (except VUCD3). In contrast to the above results we find a very significant (>99.9% significance) difference in the sizes of UCDs and early-type galaxy nuclei: the effective radii of UCDs are $2.2^{+0.2}_{-0.1}$ times larger than those of early-type galaxy nuclei at the same luminosity. This result suggests that an important test can be made of the threshing hypothesis by simulating the process and predicting what size increase is expected.

Key words: galaxies: clusters: individual (Fornax Cluster, Virgo Cluster) – galaxies: dwarf – galaxies: formation – galaxies: fundamental parameters – galaxies: star clusters – galaxies: structure

Online-only material: extended figure

1. INTRODUCTION

Ultra-compact dwarf (UCD) galaxies are a class of stellar system originally discovered in the Fornax Cluster (Hilker et al. 1999; Drinkwater et al. 2000a). They appear star-like in ground-based photographic survey images, but have recession velocities consistent with cluster membership. UCDs have spectra typical of old stellar populations but they are generally far more luminous than ordinary Milky Way (MW) globular clusters (GCs), and much more compact than similarly luminous dwarf spheroidal galaxies.

UCDs have now been detected in the Virgo (Haşegan et al. 2005; Jones et al. 2006) and Centaurus Clusters (Mieske et al. 2007) and, possibly, in Hydra I (Wehner & Harris 2007) and Abell 1689 (Mieske et al. 2004). On the other hand, they are much less common in groups (e.g., Evstigneeva et al. 2007a) and the general field (Liske et al. 2006), suggesting that UCDs are somehow related to the cluster environment. We have now surveyed the central region of the Fornax Cluster for less luminous objects: we find that the central region of the cluster contains a large population of UCDs (60 objects to a magnitude limit of $b_J = 21.5$ or roughly $M_V \sim -10.3$; Drinkwater et al. 2004; Gregg et al. 2008) although at such faint limits they clearly overlap the GC populations associated with the central cluster galaxies.

There are three main scenarios for the origin of UCDs. (1) They may simply be luminous GCs, encountered near giant elliptical galaxies because such systems often possess populous GC systems (Mieske et al. 2002). (2) A variant of this is that the bright GCs, and UCDs, may be formed via the merger of super star clusters which are abundant in nearby galaxy mergers (Fellhauer & Kroupa 2002). Presumably, the merger process is very important in the formation of bright elliptical galaxies in clusters. (3) Finally, they may be the stripped ("threshed") nuclei of former nucleated early-type dwarf galaxies, whose envelopes have been tidally removed (Bekki et al. 2001).

Part of the motivation for the stripping ("threshing") hypothesis is the similarity between UCDs and the nuclei of dwarf elliptical galaxies. Our initial study of the internal dynamical properties of UCDs (Drinkwater et al. 2003) established that the UCDs are more closely related to dwarf galaxy nuclei than to GCs. More recently we have been able to include more luminous extragalactic GCs in the analysis, suggesting that there is a continuum of dynamical properties from GCs to UCDs (Evstigneeva et al. 2007b; Hilker et al. 2007). While this supports the interpretation that UCDs are simply bright GCs,

it does not suffice to distinguish between the above three scenarios. It is only by a thorough comparison of structure, dynamics, and stellar populations (e.g., Evstigneeva et al. 2007b) between UCDs and their supposed progenitors that we can separate the main pathway of UCD formation. We need to bear in mind, however, that there may be more than one channel involved.

In this present paper, we focus specifically on the structural parameters of UCDs which can be compared to possible progenitors. The work we present here was motivated by the large sample of fainter UCDs we identified in the Fornax Cluster (Drinkwater et al. 2004; Gregg et al. 2008). This sample was ideally suited to a *Hubble Space Telescope* (*HST*) "snapshot" program, allowing us to obtain images of a statistically useful subset of our entire sample. Our primary aim was to test the first and the third hypotheses above by direct comparison of UCD structural parameters with GCs and galaxy nuclei also measured by the *HST*.

The structure of the paper is as follows. In Section 2, we describe the data sample and in Section 3 we describe the *HST* imaging and image modeling. In Section 4, we present analysis of the structure and colors of the most extensive and complete sample of UCDs in the Fornax and Virgo Clusters observed to date. The sample includes six Virgo UCDs initially presented by Evstigneeva et al. (2007b), as we have made several improvements to the image analysis. In Section 5, we summarize our results and findings. Throughout this paper we adopt distance moduli of 30.92 for the Virgo Cluster and 31.39 for the Fornax Cluster (Freedman et al. 2001), corresponding to the distances of 15.28 Mpc to Virgo and 18.97 Mpc to Fornax.

2. UCD GALAXY SAMPLE

In this section, we briefly describe the properties we use to define UCD galaxies and how we obtained the sample for our *HST* observations. More details are given in the respective discovery papers listed below.

2.1. Definition of the UCD Galaxy Type

As noted above, the UCD galaxies originally discovered in the Fornax Cluster were unresolved in ground-based photographic imaging, but had redshifts consistent with cluster membership. The first UCDs found were much more luminous than any known GCs, with apparent magnitudes in the range $17.7 < b_J < 19.7$ (Drinkwater et al. 2000a) or $-13.4 < M_V < -11.9$. At these luminosities, the UCDs were clearly distinct from any known galactic or stellar system (Drinkwater et al. 2003). Note that, although the "unresolved" criterion depends on the image quality, there is a very large gap in parameter space between the UCDs and normal dwarf galaxies, so it only serves to remove clearly normal galaxies from the samples. We have since extended our searches to fainter limits ($b_J < 21.5$ or roughly $M_V < -10.3$ in the Fornax Cluster; Drinkwater et al. 2004; Gregg et al. 2008), at these limits there is a clear overlap with objects that would normally by classified as GCs.

For the purposes of the current discussion we will use the term "UCD" to include all the compact (i.e., unresolved in our ground-based photographic imaging) intra-cluster objects we have discovered in the Virgo and Fornax Clusters, recognizing that there is clear overlap at the fainter limits with objects conventionally classified as GCs.

2.2. UCD Targets

As noted above, our *HST* snapshot proposal was motivated by the availability of a large sample of UCDs with a range of luminosities from the Fornax and Virgo Clusters. Although the UCDs were originally discovered (Drinkwater et al. 2000a) through the "all-object" approach of the Fornax Cluster Spectroscopic Survey (Drinkwater et al. 2000b), our subsequent UCD searches were more selective. In particular, we imposed color selection to avoid the reddest stellar objects as none of the original UCDs was this red.

In the Virgo Cluster, we carried out a targeted search specifically aimed at detecting *luminous* UCDs with similar properties to the originally discovered Fornax UCDs. This was very successful with nine UCDs detected in just a few hours of observing time (Jones et al. 2006). The Virgo objects were selected in the magnitude range $16.0 < b_J < 20.2$ (roughly $-15.3 < M_V < -11.1$) and the color range $b_J - r_F < 1.6$ (roughly $V - I < 1.5$). Our spectroscopic observations in Virgo were about 65% complete, so we estimate the true population of bright UCDs in the central 1 degree (∼270 kpc) radius region of the Virgo Cluster to be about 14.

In the Fornax Cluster, we extended the search to much fainter limits using very similar approach. In our final observations with the Two-Degree Field (2dF) system, we selected unresolved objects in the magnitude range $16.0 < b_J < 21.5$ (roughly $-15.8 < M_V < -10.3$) and the color range $b_J - r_F < 1.7$ (roughly $V - I < 1.6$) and we limited the area searched to a 0.9 degree radius from the center of the Fornax Cluster. This approach was again very successful with a total of 60 UCDs detected in these limits (Gregg et al. 2008). Allowing for the incompleteness of our spectroscopic observations, we estimate the true population of UCDs in the central 0.9° (∼300 kpc) region of the Fornax Cluster to be about 105. Note that this is to a fainter limit ($b_J < 21.5$) than our Virgo sample ($b_J < 20.2$).

In both cases, we only selected targets that were classified as unresolved or merged with another object from our ground-based photographic survey imaging (see Drinkwater et al. 2000b). At these magnitudes most "merged" objects consisted of a stellar object with one or more faint companions. This selection would not remove any UCDs from the samples.

We selected 50 of the known Fornax and Virgo UCDs to observe with *HST*. The targets were chosen to cover a range of luminosities, as well as avoiding overlap with our previous observations of the first Fornax UCDs (program 8685). One object from this earlier program was reselected: Fornax UCD3. We chose to re-observe this object because of its complex morphology we hoped to better resolve with the new observations.

3. *HST* OBSERVATIONS AND IMAGE MODELING

We obtained images of 21 of the requested Fornax and Virgo UCDs in the course of *HST* snapshot program 10137. The data were taken with the Advanced Camera for Surveys (ACS), High Resolution Channel (HRC), through the F606W and F814W filters. Exposure times were 870 s in F606W and 1050 s in F814W. The HRC scale is 0.025″ pixel^{-1}. For the image analysis we used MULTIDRIZZLE[9] (*.mdz) files retrieved from the *HST* archive.

[9] See http://stsdas.stsci.edu/multidrizzle.

Table 1
UCD Photometry

Object	R.A. (J2000) (h:m:s)	Decl. (J2000) (° : ′ : ″)	$m_{V,0}$ (mag)	$M_{V,0}$ (mag)	$(V-I)_0$ (mag)	$R_{\rm eff}$ (pc)	$M_{V,0}^{\rm mod}$ (mag)	ϵ
UCD3	3:38:54.10	−35:33:33.6	18.06	−13.33	1.25	86.5 ± 6.2	−13.55	0.07/0.07[a]
UCD6	3:38:05.09	−35:24:09.6	18.81	−12.58	1.07	10.3 ± 0.9	−12.54	0.12
UCD16	3:36:47.74	−35:48:34.1	20.31	−11.08	1.02	6.4 ± 0.5	−11.21	0.28
UCD17	3:36:51.68	−35:30:38.9	20.53	−10.86	0.89	11.8 ± 0.1	−10.91	0.15
UCD21	3:37:38.29	−35:20:20.6	20.90	−10.49	0.94	7.0 ± 0.1	−10.51	0.11
UCD33	3:38:17.61	−35:33:02.8	20.31	−11.08	0.88	11.4 ± 0.0	−11.04	0.08
UCD41	3:38:29.04	−35:22:56.5	19.89	−11.50	1.12	6.9 ± 0.3	−11.58	0.05
UCD43	3:38:39.34	−35:27:05.8	20.63	−10.76	1.06	5.8 ± 0.1	−10.67	0.18
UCD48	3:39:17.72	−35:25:30.2	20.11	−11.28	1.19	5.1 ± 0.5	−11.51	0.17
UCD50	3:39:34.78	−35:53:44.2	20.15	−11.24	0.93	10.9 ± 0.7	−11.30	0.32
UCD52	3:40:19.94	−35:15:29.8	20.52	−10.87	1.07	8.7 ± 0.4	−10.99	0.19
UCD54	3:40:37.11	−34:58:40.0	20.58	−10.81	0.93	4.0 ± 0.3	−10.62	0.16
UCD55	3:41:35.88	−35:54:57.8	20.30	−11.09	0.97	9.3 ± 0.3	−11.12	0.05
VUCD1	12:30:07.61	+12:36:31.1	18.68	−12.24	1.01	11.2 ± 0.2	−12.21	0.07
VUCD2	12:30:48.24	+12:35:11.1	18.69	−12.23	1.05	13.1 ± 0.8	−12.23	0.18/0.08[a]
VUCD3	12:30:57.40	+12:25:44.8	18.33	−12.59	1.27	20.0 ± 1.5	−12.65	0.16
VUCD4	12:31:04.51	+11:56:36.8	18.67	−12.25	0.99	23.2 ± 1.4	−12.30	0.16
VUCD5	12:31:11.90	+12:41:01.2	18.60	−12.32	1.13	17.8 ± 0.3	−12.32	0.01
VUCD6	12:31:28.41	+12:25:03.3	18.85	−12.07	1.07	17.4 ± 2.4	−12.11	0.04
VUCD7	12:31:52.93	+12:15:59.5	17.50	−13.42	1.17	93.2 ± 13.1	−13.43	0.12/0.05[a]
VUCD8	12:32:14.61	+12:03:05.4	18.97	−11.95	1.06	23.5 ± 2.5	−11.96	0.16
Reanalyzed *HST*/STIS data for bright Fornax UCDs from Evstigneeva et al. (2007b)								
UCD1	3:37:03.30	−35:38:04.6	19.20	−12.19	1.17[b]	22.4	−12.17	0.19
UCD2	3:38:06.33	−35:28:58.8	19.12	−12.27	1.10[b]	23.1	−12.28	0.01
UCD4	3:39:35.95	−35:28:24.5	18.94	−12.45	1.07[b]	29.5	−12.51	0.05
UCD5[c]	3:39:52.58	−35:04:24.1	19.40	−11.99	0.99[b]	25.0	−12.02	0.24/0.16[a]

Notes. The V-band apparent magnitude, $m_{V,0}$, is determined as described in Section 3 and is corrected for foreground dust extinction (Schlegel et al. 1998). The absolute magnitude, $M_{V,0}$, is computed assuming distance moduli of 31.39 and 30.92 mag for the Fornax and Virgo Clusters, respectively (Freedman et al. 2001). The $(V-I)_0$ color is reddening-corrected. The half-light radius value, $R_{\rm eff}$, is the mean of the two passbands, V and I. The $R_{\rm eff}$ and $M_{V,0}^{\rm mod}$ values were obtained from generalized King (or standard King) models for one-component UCDs and King+Sérsic models for two-component UCDs (see Section 3). The ellipticity value, ϵ, is the best model value (see the last column of Table 2), mean of the two passbands.

[a] The first number is for the core, and the second number is for the halo.

[b] The colors are from Karick et al. (2008).

[c] The difference to the analysis in Evstigneeva et al. (2007b) is that we now derive $R_{\rm eff}$ and $M_{V,0}^{\rm mod}$ from a generalized King model. It gives the more stable estimate for $R_{\rm eff}$ than the two-component King+Sérsic model obtained in Evstigneeva et al. (2007b).

To measure the total magnitudes, we plotted curves of growth (integrated magnitude versus circular aperture radius) to find an aperture radius large enough to enclose all the light from an object. The instrumental F606W and F814W magnitudes were transformed into Landolt V- and I-band following Sirianni et al. (2005). The resulting V magnitudes and $V-I$ colors are listed in Table 1.

The images of Fornax and Virgo UCDs were modeled using the two-dimensional fitting algorithm GALFIT (Peng et al. 2002) and assuming empirical King, Sérsic, and Nuker models for the luminosity profile.

The empirical King profile is characterized by the core radius, R_c, and the tidal radius, R_t, and has the following form (Elson 1999):

$$I(R) = I_0 \left[\frac{1}{(1+(R/R_c)^2)^{\frac{1}{\alpha}}} - \frac{1}{(1+(R_t/R_c)^2)^{\frac{1}{\alpha}}} \right]^{\alpha}, \quad (1)$$

where I_0 is the central surface brightness (SB). We tried both the standard model with $\alpha = 2$ and generalized model with variable α.

The Sérsic power law has the following form (Sérsic 1968):

$$I(R) = I_{\rm eff}\ \exp\left[-k \left(\left(\frac{R}{R_{\rm eff}} \right)^{\frac{1}{n}} - 1 \right) \right], \quad (2)$$

where $R_{\rm eff}$ is the half-light (effective) radius, $I_{\rm eff}$ is the SB at the effective radius, n is the concentration parameter ($n = 4$ for de Vaucouleurs profile and $n = 1$ for exponential profile) and k is a constant which depends on n.

The Nuker law is as follows (Lauer et al. 1995):

$$I(R) = I_b\ 2^{\frac{\beta-\gamma}{\alpha}} \left(\frac{R}{R_b} \right)^{-\gamma} \left[1 + \left(\frac{R}{R_b} \right)^{\alpha} \right]^{\frac{\gamma-\beta}{\alpha}}. \quad (3)$$

It is a double power law, where β is the outer power law slope, γ is the inner slope, and α controls the sharpness of the transition (at the "break" radius R_b) from the inner to the outer region. $I_b = I(R_b)$.

The UCDs are barely resolved—even with the *HST*/ACS resolution—so to obtain their intrinsic luminosity profiles, we must correct for the telescope point-spread function (PSF).

Table 2
UCD Structural Parameters

Object	Sérsic	Generalized King[a]				Nuker[b]			Best model[c]
	n	$\mu_{V,0}$[d]	R_c[e]	c[f]	α	R_b[e]	β	γ	
UCD3[g]	2.12 ± 0.36	15.43	3.58 ± 0.16	1.68 ± 0.04	2.00 ± 0.00	...	...	...	K+S, S+S
UCD6	3.70 ± 0.18	13.62	$2.57^{h} \pm 0.25$	2.31 ± 0.11	3.34 ± 0.18	3.94 ± 0.10	2.77 ± 0.06	0.17 ± 0.04	N, GK
UCD16	5.17 ± 0.08	13.22	$1.06^{h} \pm 0.04$	2.54 ± 0.16	3.00 ± 0.50	...	...	...	GK, N, S, K
UCD17	1.08 ± 0.04	16.73	7.72 ± 0.21	0.91 ± 0.03	2.00 ± 0.00	37.41 ± 1.65	8.86 ± 0.01	0.01 ± 0.01	N, S, K
UCD21	1.35 ± 0.01	15.95	3.77 ± 0.01	1.07 ± 0.01	2.00 ± 0.00	20.94 ± 0.53	7.40 ± 0.01	0.21 ± 0.02	N, S, K, GK
UCD33	1.30 ± 0.04	16.30	6.89 ± 0.16	1.16 ± 0.02	2.77 ± 0.01	12.57 ± 0.68	3.80 ± 0.13	0.32 ± 0.01	N, GK, S, K
UCD41	3.85 ± 0.01	13.72	$1.30^{h} \pm 0.06$	1.78 ± 0.01	1.30 ± 0.05	...	...	...	GK, S, K
UCD43[g]	5.92 ± 1.67	13.51	$0.56^{h} \pm 0.06$	1.85 ± 0.12	2.00 ± 0.00	10.68 ± 1.00	2.76 ± 0.28	1.68 ± 0.06	K+S, N, S, GK
UCD48	8.24 ± 0.43	11.58	$0.47^{h} \pm 0.07$	2.33 ± 0.08	1.10 ± 0.10	34.37 ± 1.80	3.65 ± 0.08	1.76 ± 0.02	N, GK, S, K
UCD50	3.25 ± 0.07	14.79	2.84 ± 0.06	2.29 ± 0.06	3.56 ± 0.04	8.43 ± 0.01	3.68 ± 0.05	0.00 ± 0.00	N, K, GK
UCD52	4.21 ± 0.02	14.52	$1.56^{h} \pm 0.06$	1.82 ± 0.08	1.28 ± 0.23	15.39 ± 1.15	2.87 ± 0.07	1.42 ± 0.06	N, S
UCD54	3.47 ± 0.26	13.87	$0.78^{h} \pm 0.19$	1.73 ± 0.01	1.14 ± 0.41	...	...	...	N, S, K, GK
UCD55	2.15 ± 0.06	15.57	3.49 ± 0.09	1.57 ± 0.03	2.55 ± 0.28	8.90 ± 0.57	3.88 ± 0.04	0.01 ± 0.00	K, GK, S, K
VUCD1	2.23 ± 0.11	14.67	4.28 ± 0.11	1.92 ± 0.06	3.74 ± 0.03	6.25 ± 0.14	2.69 ± 0.03	0.23 ± 0.00	N
VUCD2[g]	1.11 ± 0.10	15.09	5.16 ± 0.12	0.94 ± 0.04	2.00 ± 0.00	7.56 ± 0.07	2.61 ± 0.06	0.54 ± 0.01	K+S, S+S
VUCD3	8.27 ± 0.06	13.80	2.10 ± 0.15	2.06 ± 0.00	0.62 ± 0.01	...	...	...	S, N
VUCD4[g]	1.11 ± 0.11	16.01	7.52 ± 0.09	0.96 ± 0.05	2.00 ± 0.00	9.08 ± 0.16	2.35 ± 0.04	0.32 ± 0.04	N, K+S, S+S
VUCD5	1.91 ± 0.04	15.97	6.56 ± 0.01	1.42 ± 0.01	2.00 ± 0.00	18.21 ± 1.39	3.92 ± 0.16	0.00 ± 0.00	K, N
VUCD6[g]	1.16 ± 0.11	15.26	4.08 ± 0.06	0.96 ± 0.02	2.00 ± 0.00	5.21 ± 0.35	2.24 ± 0.04	0.50 ± 0.06	N, K+S, S+S
VUCD7[g]	2.18 ± 0.10	14.38	3.09 ± 0.04	1.62 ± 0.04	2.00 ± 0.00	...	...	...	K+S, S+S
VUCD8	4.07 ± 0.22	15.41	3.33 ± 0.04	2.01 ± 0.08	1.28 ± 0.00	3.69 ± 0.11	2.24 ± 0.04	0.00 ± 0.00	N, K, GK

Notes. All the parameters (except $\mu_{V,0}$) are the means of the two passbands, V and I.
[a] If the standard King model ($\alpha = 2.0$) fits the object better than the generalized King model (α is a free parameter), we provide parameters for the standard King model.
[b] The Nuker model parameters are provided only if this model is reasonably good for the object and there is a good agreement between two passbands.
[c] N: Nuker, K: King ($\alpha = 2$), GK: generalized King (α: any), S: Sérsic, K+S: King plus Sérsic, S+S: Sérsic plus Sérsic.
[d] $\mu_{V,0}$ is measured in mag arcsec^{-2}.
[e] R_c and R_b are measured in pc.
[f] Concentration $c = \log(R_t/R_c)$.
[g] For two-component UCDs, Sérsic and King model parameters are given for the central (core) component.
[h] $R_c < 1$ pix, core is unresolved.

We derived artificial PSFs for the images in each filter using the TinyTim software[10] and MultiDrizzle as described in Evstigneeva et al. (2007b). The size of the PSFs was chosen to be $3.5'' \times 3.5''$ (140×140 pixel), slightly larger than the minimum size recommended by TinyTim. For the brightest UCDs, which are also the most extended, we used PSFs of a larger size (the same as for the color gradient analysis in Section 4.3.1) to correct for the extended PSF halo in the F814W filter.

GALFIT models an analytic profile convolved with the PSF and determines the best-fitting profile parameters by minimizing residuals between the model and original two-dimensional image. We limited all the models to a maximum fitting radius defined by the point where the UCD light profile reaches the background noise level in the V image (the models are not constrained beyond that point). The image of Fornax UCD3 is complicated by the presence of a background object in projection (possibly a spiral galaxy, see Evstigneeva et al. 2007b). We therefore restricted the model fitting to the half of the image least affected by the background source.

The sky (background) was estimated and subtracted from the UCD images before running GALFIT. The sky was initially subtracted by MultiDrizzle. We then applied additional background corrections, determined from empty parts of the images. So we held the sky value fixed to zero when fitting the images. It is important to hold the sky fixed when fitting standard models to an object, because the model function used may not be optimal and the model mismatch can push the sky around a little. On the other hand, if the object is fitted as well as possible (by multi-component models) and if the sky region is large enough to fit, then the sky can be allowed to vary as a free parameter. This is what we did for the color gradient analysis in Section 4.3.1. Thus, in this section, for the structural modeling, we held the sky value fixed (did not fit the sky with GALFIT). We, however, did the tests of changing the sky by hand (subtracting the sky values found by GALFIT in Section 4.3.1) and redoing the fit. It did not affect the structure parameters in Tables 1 and 2 very much: the changes were within the uncertainties given in the tables. However, the sky corrections can be critical for the outer color profile, for the tiny color gradients we find in UCDs.

The quality of the GALFIT model fits is shown in Figure 1. For this figure, we used the ELLIPSE task in IRAF to produce one-dimensional SB profiles for the objects and (PSF-convolved) GALFIT models.

To choose the *best model* for each object (see the last column of Table 2), we used χ^2_ν values of the fits (Peng et al. 2002). In the case of faint UCDs ($m_{V,0} \sim 19.9$–20.9 mag), there is no preference of one model over another: all the models (Nuker, King, and Sérsic) seem to fit the UCDs equally well within the errors. The bright UCDs ($m_{V,0} \sim 17.5$–18.9 mag) have extended outer halos and appear to be best fitted by a double power law (Nuker) or two-component models (the central component was fitted by King with $\alpha = 2$ or Sérsic and the outer

[10] See http://www.stsci.edu/software/tinytim.

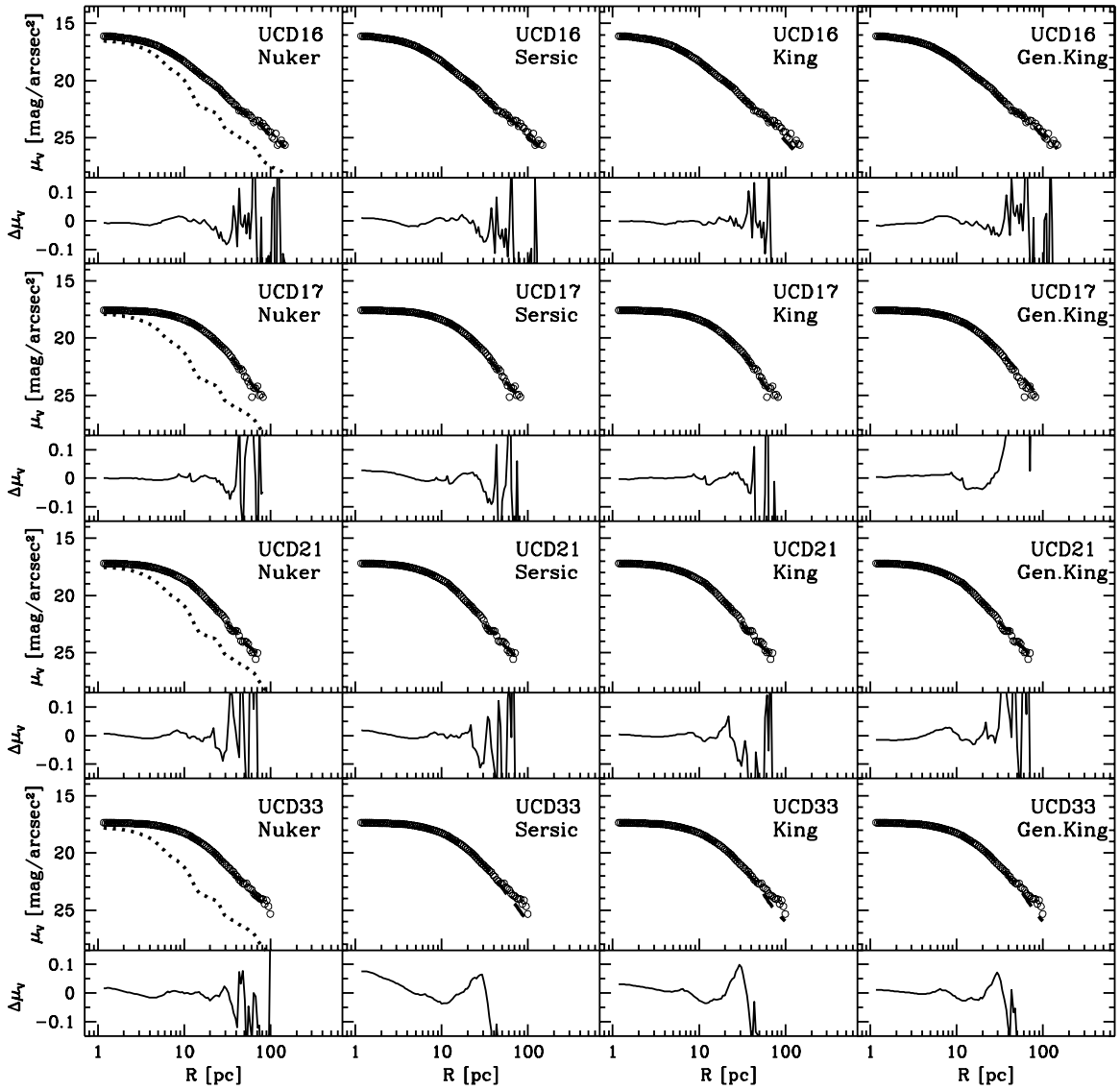

Figure 1. SB profiles, measured in the F606W images, and model fits to four UCDs. The plots for the other seventeen UCDs are available in the online version of this paper (Figures 1.1.–1.5). The magnitudes are AB magnitudes. The open circles represent the UCD profile, the dashed line represents the best-fitting model, convolved with the PSF. The PSF for each object is shown with the dotted line. $\Delta\mu_V$ plots show the residuals for each fit: the difference (in magnitudes) between the UCD profile and the profile of the best-fitting model, convolved with the PSF.

(An extended version of this figure is available in the online journal)

envelope by Sérsic). This does not necessarily mean that bright and faint UCDs are intrinsically different. If we had deeper observations for the fainter UCDs, we would possibly be able to detect outer halos in them were any present. The detection of extended halos around the luminous UCDs is not consistent with their having the standard King profiles traditionally associated with GCs, but recent work of McLaughlin & van der Marel (2005) and McLaughlin et al. (2008) has shown that extended halos are a general characteristic of massive GCs in the MW and some of its satellites and NGC 5128.

In Table 1 we quote effective radius $R_{\rm eff}$, model magnitude $M_{V,0}^{\rm mod}$, and ellipticity ϵ. The ellipticity value is the best model value (see the last column of Table 2). The $R_{\rm eff}$ and $M_{V,0}^{\rm mod}$ values were obtained from generalized King (or standard King with $\alpha = 2$, if it fits better) models for one-component UCDs and King+Sérsic models for two-component UCDs, via numerical integration (to infinity) of the V and I luminosity profiles. These models give the most stable estimates for $R_{\rm eff}$ as discussed in Evstigneeva et al. (2007b). The $M_{V,0}^{\rm mod}$ values are only slightly different from the observational $M_{V,0}$ values, obtained by integrating the actual image pixel values. In further analyses we use observational magnitudes ($M_{V,0}$). The choice of magnitude, however, does not change our final results and conclusions (e.g., Equations (4)–(7) stay the same, as well as the size difference between UCDs and nuclei, found below). Table 1 also contains the parameters for the four bright Fornax UCDs from Evstigneeva et al. (2007b) (*HST*/STIS data), as we have made some improvements to the image analysis and we use these data in the analyses below.

In Table 2 we list more model parameters such as Sérsic index n; King central SB $\mu_{V,0}$, core radius R_c, concentration c and α parameter; Nuker inner slope γ, outer slope β, and break radius R_b. We do not list all the parameters for all the models, but only the most significant ones needed for qualitative analysis, mainly to compare UCDs with each other. We recommend caution in using the actual values of these parameters in detailed analyses.

One of the main reasons for this is that the objects are barely resolved. For example, for about half of the UCDs, the King model fits appear good, but the core radii of these models $R_c < 1$ pixel. It means that these UCDs either have cores, which are unresolved, or do not have cores at all, so that the actual R_c values are uncertain. As a result, we cannot trust the values of central SB and concentration obtained from these King models. The central SB of UCDs can also be derived from Sérsic models: we can calculate $\mu_{V,0}$ from GALFIT's $m_{V,\mathrm{tot}}$, R_{eff}, and n values analytically by using formulae for the Sérsic function. However, for models with high Sérsic indices ($n > 2$), the calculations result in unrealistically high central SB values. As for the Nuker parameters, they are not always stable. If we change the radial extent to which we fit this model, there is a good chance that all the parameters will change considerably (Graham et al. 2003).

4. ANALYSIS AND DISCUSSION

4.1. Structural Parameters

The results of the modeling show that the UCDs have a range of Sérsic indices n and King concentrations c, as well as a range of central slopes (seen from Nuker inner slopes γ): from flat "King" cores to central cusps. This suggests that convolving some cuspy models with the PSF allows such models to fit the seeing-blurred centers of some UCD profiles. We, however, cannot make very strong conclusions regarding central cusps or cores in the UCDs, taking into account the limits of our data (described in the previous section).

We tried to look for correlations of the model parameters in Table 2 with the UCD luminosity, size, and color, but did not find any.

We compared the distribution of UCD ellipticities (in Table 1) with those for MW GCs (Harris 1996), NGC 5128 GCs (Holland et al. 1999; Harris et al. 2002), and M31 GCs (Barmby et al. 2007). The two-sample K-S test shows that the UCD ellipticities are consistent with extragalactic GC distributions (NGC 5128 and M31 GCs), but significantly different from the MW GC distribution. The Wilcoxon test gives the same result. It is interesting to note that Harris et al. (2002) found the MW GC ellipticity distribution to be significantly different from the NGC 5128 and M31 GC distributions. Harris et al. (2002), however, do not place too much weight on their result because of uncertainties about possible selection effects and different methods for ellipticity measurements (see also Barmby et al. 2007).

No correlation of ellipticity with luminosity, size, or color was found for UCDs.

In Figure 2, we present the luminosity–size diagram for UCDs. For comparison, we also show "dwarf globular transition objects" from Haşegan et al. (2005), early-type galaxy nuclei from Côté et al. (2006) and GCs (see the caption of Figure 2). The UCDs and GCs form a continuous distribution across the plane, but UCDs seem to be different to *typical* GCs in the sense that the UCDs have sizes correlated with luminosities whereas the GCs do not. This difference has been reported previously (e.g., by Haşegan et al. 2005 for "dwarf globular transition objects" and five bright Fornax UCDs).

We obtain the following luminosity–size relation for the UCDs in our sample (fitting a linear least-squares regression to the data for both Fornax and Virgo UCDs in Table 1):

$$\log R_{\mathrm{eff}} = -3.03(\pm0.55) - 0.35(\pm0.05)\, M_V \qquad (4)$$

$$\text{or} \quad R_{\mathrm{eff}} \propto L_V^{0.88\pm0.13}. \qquad (5)$$

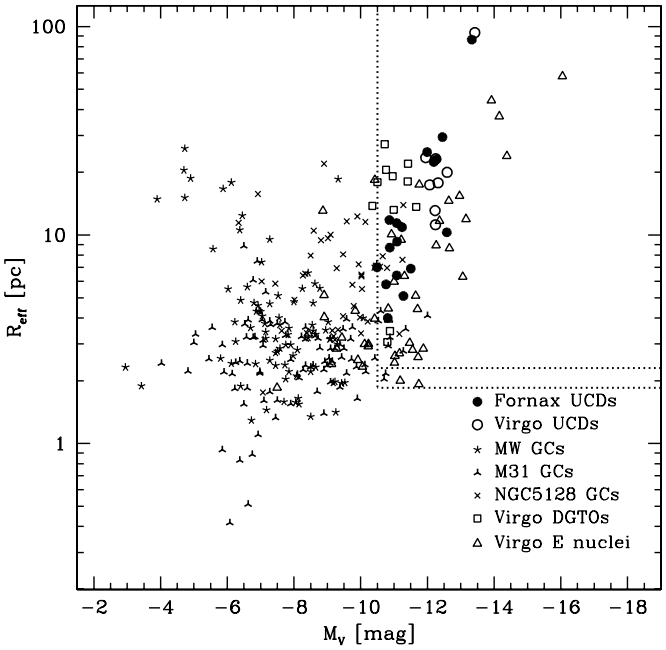

Figure 2. Luminosity–size diagram. Fornax and Virgo UCDs: this work (Table 1). MW GCs: McLaughlin & van der Marel (2005), photometry is based on Wilson models. M31 GCs: Barmby et al. (2007), photometry is based on King models. NGC 5128 GCs: Holland et al. (1999), Harris et al. (2002). Virgo DGTOs: Haşegan et al. (2005), certain DGTO candidates, R_{eff} is the mean of the two passbands, g' and z'. Virgo early-type galaxy nuclei: Côté et al. (2006), all resolved nuclei, R_{eff} is the mean of the two passbands, g' and z'. The vertical dotted line shows the magnitude limit of our 2dF/*HST* UCD observations. The horizontal lines show the *HST*/ACS resolution limit: the lower line is for the Virgo distance and the upper line is for Fornax (below these lines $R_{\mathrm{eff}} < 1$ pix).

If we exclude the two brightest objects, which may be different from all other UCDs (they are much brighter than all other UCDs and have the largest envelopes), we obtain

$$\log R_{\mathrm{eff}} = -2.11(\pm0.61) - 0.27(\pm0.05)\, M_V \qquad (6)$$

$$\text{or} \quad R_{\mathrm{eff}} \propto L_V^{0.68\pm0.13}. \qquad (7)$$

The fact that the UCDs show a luminosity–size relation while the GCs do not is not a result of any selection effects. To illustrate this point, we show in Figure 2 the selection boundaries for our UCD sample. The sample selection is only restricted at the faint magnitude end (by our survey flux limit corresponding to $M_V = -10.5$ mag, vertical line). The size limit (horizontal lines) is an approximate representation of the minimum size that could be parameterized from *HST*/ACS imaging: below this limit objects become unresolved. It does not represent a detection limit, because the 2dF surveys were sensitive to objects regardless of their sizes. All the UCDs, however, are resolved with *HST*/ACS ($R_{\mathrm{eff}} > 1$ pixel).

The luminosity–size relation we observe for the UCDs is similar to the *bright* GC observations by Barmby et al. (2007). They report an increasing lower bound on R_{eff} in the mass versus R_{eff} plane for the most massive GCs (masses $\geqslant 1.5 \times 10^6\, M_\odot$). Barmby et al. interpreted it as an extension of a similar relation for early-type galaxies following from the existence of a "zone of exclusion" (ZOE) in the fundamental plane (κ-space), discussed by Burstein et al. (1997). According to Burstein et al. (1997), no stellar system violates the rule $\kappa_1 + \kappa_2 < 8$, which means that the maximum global luminosity density of stellar systems varies as mass$^{-4/3}$. Assuming constant mass-to-light ratios, this is equivalent to $R_{\mathrm{min}} \propto L^{0.78}$, the same relation (within

uncertainties) as we find for UCDs. So if we consider UCDs as a part of GC family, perhaps it would be more correct to talk about the increasing lower boundary on $R_{\rm eff}$ rather than about the luminosity–size relation for them, which could be explained by the ZOE. However, the existence of a ZOE for galaxies is not quite understood yet.

The nuclei of early-type galaxies also show a luminosity–size correlation as noted by Côté et al. (2006). Fitting a linear least-squares regression to all the nuclei brighter than $M_V = -10.5$ mag, except for the brightest one at $M_V \sim -16$ mag (to approximately match the UCD luminosity range), and excluding both unresolved and offset nuclei, we found the following relation:

$$\log R_{\rm eff} = -2.53(\pm0.58) - 0.28(\pm0.05)\, M_V \quad (8)$$

$$\text{or} \quad R_{\rm eff} \propto L_V^{0.70\pm0.13}, \quad (9)$$

where $R_{\rm eff}$ is the mean of the two passbands, g' and z'. This relation is very similar (especially the slope) to the UCD luminosity–size relations above. This is consistent with the threshing hypothesis for UCD formation from disrupted early-type galaxies. We do not show the nuclei of late-type galaxies (or "nuclear star clusters") in Figure 2. They are nearly identical to the early-type galaxy nuclei in the sense of luminosities and sizes (e.g., Côté et al. 2006 and references therein), so they would not add new information to the figure. The similarity, however, means that UCDs—if formed by disruption—could be the remnant nuclei of both early-type and late-type galaxies, not just dE,Ns as it was initially suggested.

From inspection of Figure 2 and the luminosity–size relations above, we note that the UCDs are significantly larger than the corresponding early-type galaxy nuclei at the same luminosity. This is consistent with an earlier comparison we made of the brighter Fornax UCDs with some fainter nuclei (de Propris et al. 2005b), but we are now able to confirm that the size difference is not due to the difference in luminosity of those samples.

Taking the luminosity–size relation fitted for the galaxy nuclei as a baseline, we calculate that the UCDs are an average factor of $\Delta \log R_{\rm eff} = 0.35 \pm 0.03$ larger (we do not include the two brightest UCDs with the largest envelopes here). This difference is significant at a confidence level $> 99.9\%$ (using the T-test) and corresponds to the effective radii of the UCDs being on average $10^{0.35\pm0.03} = 2.2^{+0.2}_{-0.1}$ times larger than the nuclei of the same luminosity. In Figure 3 we show the histograms of $R_{\rm eff}/L_V^{0.7}$ for nuclei and UCDs separately (in the same luminosity range as was used to derive relations (7) and (9)), which better emphasizes the difference between UCDs and early-type galaxy nuclei. Although this observation is superficially inconsistent with a process whereby these galaxy nuclei are stripped to form UCDs, the change in size may be a result of the stripping process. The nuclei may be more concentrated (denser) than the UCDs due to a truncation effect caused by their location within the prominent stellar envelope (or dark matter halo) of a galaxy which does not affect the isolated UCDs. Conversely, the stripping process itself may well result in dynamical heating of the nuclei, so they expand as their host galaxies are disrupted. The simulations of the stripping process by Bekki et al. (2001, 2003) do indicate some expansion of the remnant core, but no quantitative results are provided. Given our new observational result, it will be important to test this in detail against simulations of the threshing process to see if it is consistent with the size difference we have found between UCDs and the early-type galaxy nuclei. As an additional constraint

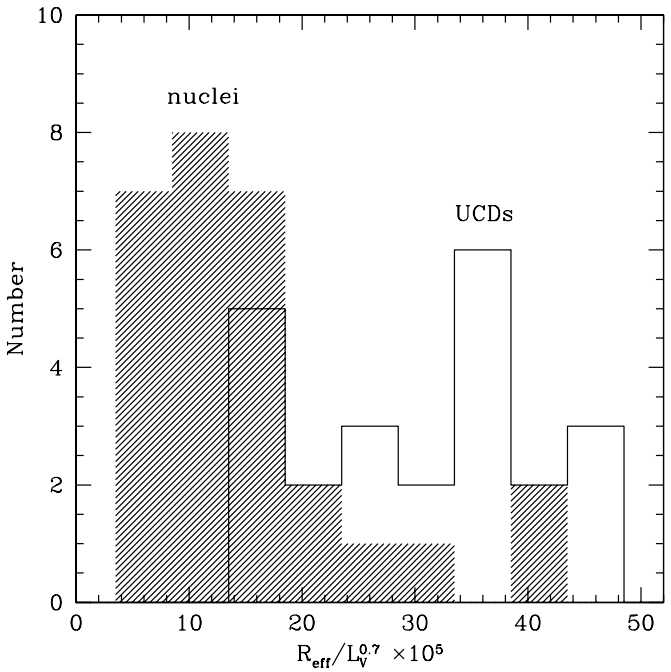

Figure 3. Size comparison of UCDs and early-type galaxy nuclei. The sizes are all scaled relative to the size–luminosity relation fitted for the nuclei in Equation (9).

on this process we note that the cores of the largest UCDs (which have small stellar envelopes) have magnitudes and sizes similar to the other UCDs (which do not have envelopes): $-11.16 \geqslant M_V \geqslant -12.39$ mag, $6.5 \leqslant R_{\rm eff} \leqslant 12.8$ pc. They are still larger on average than early-type galaxy nuclei at the same luminosity. This means that the gravitational potential of these small stellar envelopes is not be enough to squeeze the central component to the extent that the galaxy nuclei are compressed.

4.2. Color–Magnitude Diagrams

The total colors of the UCDs from our ACS survey (Table 1) can be compared to those of other hot stellar systems in the same environment. We therefore constructed color–magnitude diagrams (CMDs) for GCs, nuclei of early-type galaxies and UCDs in the Virgo and Fornax Clusters. These are shown in Figures 4 and 5. All magnitudes and colors were transformed to the Johnson–Cousins V and $(V - I)$ system to facilitate the comparison of our data to many other works in this filter set.

The GC data were taken from the ACS Virgo Cluster Survey (M87 and M49 GCs, Côté et al. 2004; Peng et al. 2006) and the ACS Fornax Cluster Survey (NGC 1399 and NGC 1404 GCs, Jordán et al. 2007). The magnitudes and colors for the nuclei of Virgo early-type galaxies and "dwarf globular transition objects" were also taken from the ACS Virgo Cluster Survey (Côté et al. 2006; Haşegan et al. 2005). The transformations from the ACS survey g' and z' AB magnitudes to the V and I magnitudes were performed by using theoretical single stellar population (SSP) models of Bruzual & Charlot (2003). We derived transformation equations for three different age bins to account for possible intermediate age populations in nuclei and "dwarf globular transition objects." For a Chabrier initial mass function (IMF) and a metallicity range of -2.2 to 0.6 dex, the transformation equations for the three age bins

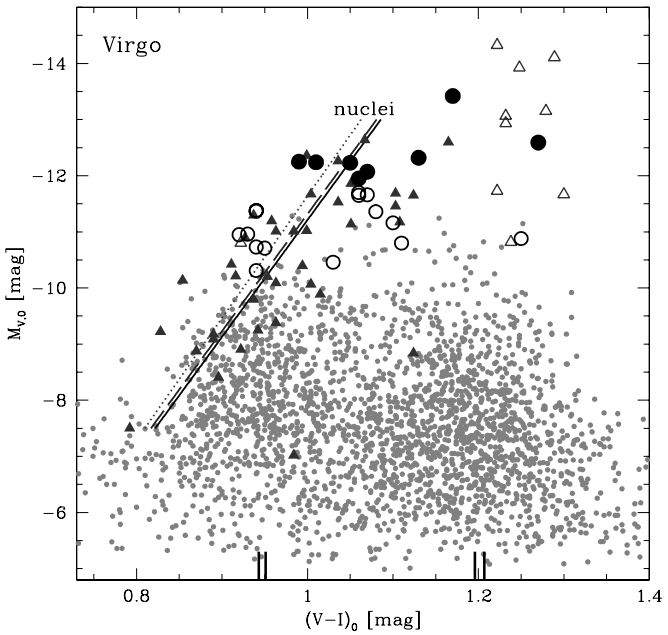

Figure 4. CMD for the Virgo Cluster objects. The filled circles are Virgo UCDs from the present work. The open circles are "certain and probable" Virgo "dwarf globular transition objects" from Haşegan et al. (2005). Grey dots are M87 and M49 GCs from the ACS Virgo Cluster Survey. Triangles are nuclei of early-type galaxies from the ACS Virgo Survey: open triangles—nuclei of galaxies brighter than $B_T = 13.5$ (approximate dividing point between dwarf and giant galaxies), filled triangles—nuclei of galaxies fainter than $B_T = 13.5$. The line is the fit to the sample of nuclei of galaxies fainter than $B_T = 13.5$ (three lines correspond to three different age bins used for magnitude transformations: solid line—11–13 Gyr, dashed line—6–8 Gyr, dotted line—2–4 Gyr). Ticks on the bottom: peak colors for the blue and red GC population of M87 and M49 from Larsen et al. (2001).

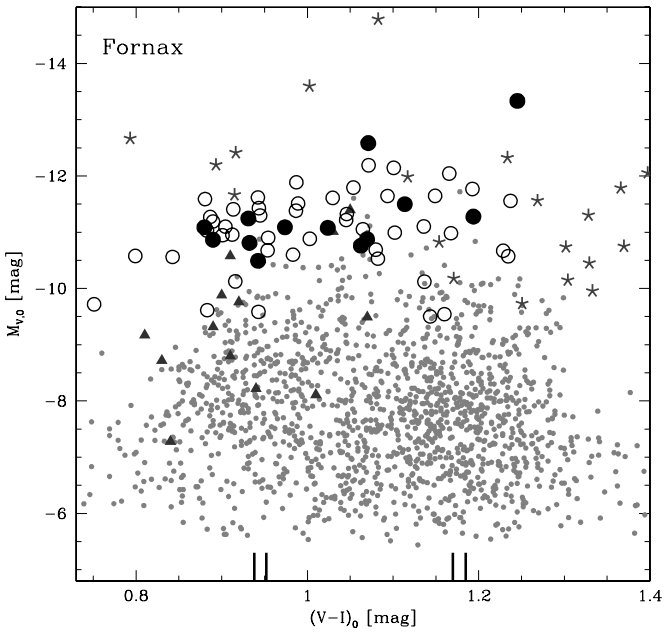

Figure 5. CMD for the Fornax Cluster objects. The filled circles are Fornax UCDs from the present work. The open circles are Fornax UCDs from Gregg et al. (2008). Grey dots are NGC 1399 and NGC 1404 GCs from the ACS Fornax Cluster Survey. The filled triangles are dwarf elliptical nuclei from Lotz et al. (2004). Ticks are for the blue and red GC peaks of NGC 1399 and NGC 1404 (Larsen et al. 2001). Asterisks are nuclear star clusters (NCs) of late-type galaxies (Rossa et al. 2006).

are as follows:

$$\text{11–13 Gyr}: \quad V_0 = g'_{AB} - 0.004 - 0.301(g' - z')_{AB} \quad (10)$$

$$(V - I)_0 = 0.445 + 0.518(g' - z')_{AB}\,; \quad (11)$$

$$\text{6–8 Gyr}: \quad V_0 = g'_{AB} - 0.005 - 0.298(g' - z')_{AB} \quad (12)$$

$$(V - I)_0 = 0.449 + 0.515(g' - z')_{AB}\,; \quad (13)$$

$$\text{2–4 Gyr}: \quad V_0 = g'_{AB} + 0.015 - 0.315(g' - z')_{AB} \quad (14)$$

$$(V - I)_0 = 0.451 + 0.496(g' - z')_{AB}\,. \quad (15)$$

For the objects in Figures 4 and 5, we chose the transformation equations obtained for the very old ages. The age effect on the transformations, however, is not strong, as shown by the color–magnitude relations for the Virgo nuclei in Figure 4, and the choice of age does not affect our main conclusions below.

The tick marks on the bottom of the CMDs in Figures 4 and 5 indicate the peak colors for the blue and red GC populations in Virgo and Fornax derived by Larsen et al. (2001). They are in a good agreement with the average transformed colors for the blue and red GCs from the ACS surveys. This shows the reliability of our transformations.

The nucleus V and $(V-I)$ values for Fornax dwarf ellipticals were taken from Lotz et al. (2004). For the Fornax UCDs, we present our ACS sample plus additional objects from Gregg et al. (2008) with colors from Karick et al. (2008): the original Sloan Digital Sky Survey (SDSS) gri magnitudes were transformed to VI via the transformation equations available at the SDSS Data Release 4 Web site.[11]

Looking at the CMDs, we observe that the UCDs and "dwarf globular transition objects" are spread over the same color range as GCs. The brightest UCDs ($M_V < -12.3$ mag), however, seem to favor red colors, thus probably are an extension of the metal-rich GC peak. Interestingly, Wehner & Harris (2007) found such an extension of red GCs toward the UCD regime in the extraordinary rich GC system of NGC 3311, the central galaxy in the Hydra I Cluster.

The apparent "gap" in luminosity for the objects around $M_V \sim -10$ mag is a pure selection and incompleteness effect. On the one hand, the GCs from the ACS surveys only cover a small area around galaxies and are selected by their apparent sizes and magnitudes. UCDs would have been rejected by these surveys as extended background galaxies. On the other hand, the redshift-selected UCDs cover a large area in the clusters but suffer from the completeness limit of spectroscopic surveys. Our Fornax Cluster survey has a magnitude limit of $M_V \sim -10.3$ mag (roughly).[12]

An additional feature is visible in the Fornax CMD. There is a group of UCDs (with $M_V \sim -10.5$ mag) which exhibit very blue colors, $V - I \leqslant 0.9$ mag. Such colors can be interpreted in two ways: either these UCDs are very metal poor ([Fe/H] ~ -2 dex), or their stellar populations are of intermediate age. Indeed, some UCDs in Fornax show increased Hβ line indices (Mieske et al. 2006), a hint to the contribution of young stellar populations.

[11] See http://www.sdss.org/dr4/algorithms/sdssUBVRITransform.html.
[12] We note that some UCDs in Figure 5 have lower luminosities than the nominal survey limit. This is because the original survey selection was based on photographic photometry with relatively high uncertainties.

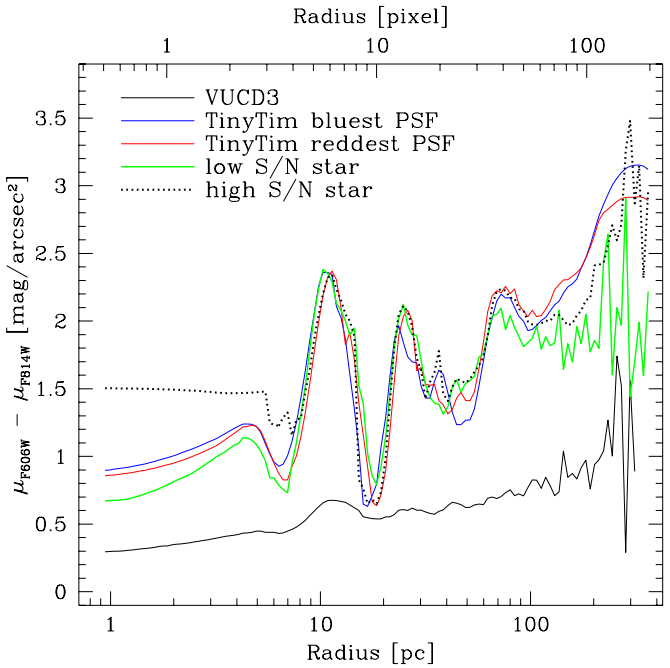

Figure 6. PSF color profiles in comparison with the VUCD3 color profile (contains all PSF effects). All the PSF profiles are normalized at ∼6 pixels (∼11 pc at the Virgo Cluster distance).

In the Virgo CMD, we plot the color–magnitude relation for dwarf galaxy nuclei (host galaxy magnitude $B_T > 13.5$ mag) from the ACS Virgo Survey (Côté et al. 2006). A large fraction of UCDs (as well as "dwarf globular transition objects") falls close to this relation. Interestingly, the nuclei of early-type giant galaxies cluster around red colors, $V - I \sim 1.25$ mag, at the same location where the brightest and also the reddest UCDs are found. We cannot distinguish UCDs from nuclei of early-type galaxies by simply using magnitudes and colors.

In the Fornax CMD, we also show nuclear star clusters (NCs) of late-type galaxies, although the galaxies are not Fornax members. The data are from the work of Rossa et al. (2006), based on previous works by Walcher et al. (2005, 2006) and Böker et al. (2002, 2004). The data were corrected for the foreground extinction but the intrinsic extinction of the host galaxy is more problematic. Only few NCs in the Rossa et al. and Böeker et al. lists have estimates of the internal reddening (and were corrected for it). As we mentioned in the previous section, NCs of late-type galaxies and nuclei of early-type galaxies are nearly identical in the sense of luminosities and sizes. The only difference is that the majority of NCs have young ages, they are younger than early-type galaxy nuclei. Looking at Figure 5, one can see that there are some blue (young) NCs that are close to the location of blue GCs and UCDs or at least should pass this location when aging. There are quite a few NCs with very blue colors ($V - I < 0.7$ mag) and bright magnitudes ($M_V < -10$ mag), which cannot be seen in Figure 5 due to the scale of the figure. There are also many red NCs that probably are contaminated by internal reddening (so they might actually be bluer). The blue NCs look very bright, on average brighter than early-type galaxy nuclei and UCDs. The bright magnitudes can be caused by young ages. Younger stellar populations are not only bluer but also much brighter. They will fade with time. Red bright NCs might be intrinsically very luminous/massive. They come mostly from MW-type spirals. As above (in Section 4.1), the main conclusion we can draw out of the comparison of UCDs with NCs is that some of the UCDs, both blue and red, could be threshed nuclei of late-type galaxies.

4.3. Color Profiles and Color Gradients

The analysis of radial color gradients for the UCDs is very challenging, mainly because they are tiny and very compact objects, hardly resolved even with the *HST*. So the corrections for telescope PSF effects become extremely important. In this section, we therefore reanalyze the images to obtain the best possible estimates of the radial color profiles and devise a series of tests to quantify how the PSF and other issues affect the color profiles. Note that we present results for the brightest UCDs only (Virgo UCDs and Fornax UCD3 and UCD6) as the color gradients for the fainter UCDs could not be estimated with any reliability.

4.3.1. Measurement of Color Gradients

We obtain the radial color profiles by fitting UCD images with PSF-convolved models using GALFIT. Superficially, it may appear easier to derive color profiles directly from PSF-deconvolved images. However, we choose not to do this, as a deconvolution process (e.g., the Lucy–Richardson algorithm) amplifies noise in the image and, in our case, produces very large artificial fluctuations in the color profiles. Instead we derive color profiles from GALFIT models. We do not use the models obtained in Section 3 as these were designed to obtain the best parameters for standard models where possible. The differences to the approach in Section 3 are as follows.

1. Multiple component models (e.g., King+Sérsic+Sérsic) are used to better fit the UCDs. No constraints that the model parameters must have physically meaningful values are applied. Our aim is to match the UCD SB profiles as well as possible. Multiple Sérsic models are the best for almost all the UCDs.
2. The PSFs are presented out to a radius of 10″ in the modeling. We also do several experiments with the PSFs to make sure that the color gradients we find for UCDs are robust.
3. We fit the background directly rather than holding it fixed.

We start by using GALFIT to fit more general multi-component models to each UCD and filter combination. From the best-fitting parameters we generate the two-dimensional model (using GALFIT again), which is in principle free of PSF effects. Then we calculate SB profiles for the models in each filter using the IRAF task ELLIPSE. The color profile is then determined as the difference of the SB profiles in the two filters. The resulting color profiles are presented in the top panels of Figures 7–16.

In the rest of this subsection we discuss the most important issues which affect the color profiles, such as the accuracy of the GALFIT model fits to the data, PSF effects, and sky subtraction.

1. Accuracy of the GALFIT *model fits to the data*. The object-minus-model residuals are shown in the bottom panels of Figures 7–16. The residuals get larger with radius. This is normal and expected. If we plot the error bars on the UCD SB profiles produced by ELLIPSE (errors on measuring the mean flux along each isophote), we find that they are comparable to the size of the residuals. The most important point here is to fit the objects so that the residuals do not show any systematic trend (so that the residuals fluctuate evenly around zero). In some cases, the

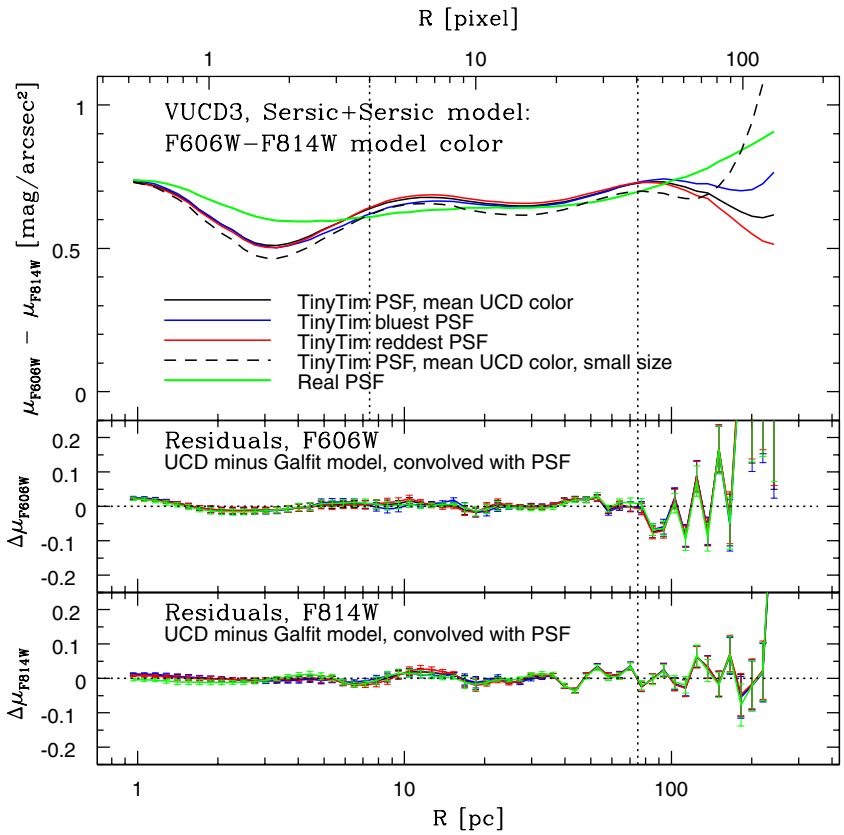

Figure 7. VUCD3 color profile.

residual fluctuations are larger than the ELLIPSE errors, but this could be because the ELLIPSE error bars are only statistical and do not include any other possible errors.

2. PSF effects. The PSF depends on the object color. In the same broadband filter, the PSF (PSF FWHM) of a red star may be noticeably larger than that of a more blue star. We therefore generated three PSFs using TINYTIM (and MULTIDRIZZLE, as described in Section 3): one with the average UCD color, one with the reddest, and one with the bluest possible with TINYTIM color.

The PSFs were made of a very large size ($20'' \times 20''$ or 800×800 pixel, larger than the UCDs) to attempt to address the PSF halo problem. The ACS/HRC chip has a defect that creates a halo surrounding the PSF at wavelengths > 0.6 μm and the relative proportion of flux within this halo increases with wavelength. The halo is large (many arcseconds) and can contain 10–20% of the total flux. TINYTIM models this effect, but unfortunately not very well.[13]

Stellar images ("real" PSFs) are better representations of the *true* PSF, but they also have some disadvantages. All the stellar images we found in the *HST* archive suitable for the UCD image modeling (i.e. images of a single star which was centrally located and non-saturated) are much bluer than the UCDs. Another disadvantage of these PSFs is that they have a very low signal-to-noise ratio (S/N) at large radii and, therefore, cannot correctly capture the outer PSF halo. Brighter stars, which have higher S/N at large radii, are saturated in the center and, hence, cannot be used for modeling, but we can use them for the comparison with the TINYTIM PSFs, to check how reliable the TINYTIM PSFs are at large radii. We have managed to find in the archive a couple of high S/N stars with red colors, similar to UCD colors.

In Figure 6 we plot the color profiles for TINYTIM PSFs, a low S/N star (with blue color), and a high S/N star (with red color), and normalize all of them at $\sim$ 6 pixels. All TINYTIM PSFs look very similar (except at very large radii, $R > 100$ pixels) and give very similar results for the UCD color profiles in Figures 7 and 8. So for the UCD image modeling, we can safely use just one TINYTIM PSF with the average UCD color. Another important conclusion we can draw from Figure 6 is that the color profiles of the high S/N star (with red color similar to UCD colors) and TINYTIM PSFs are nearly the same in the region $\sim$ 4–54 pixels. The match between the color profiles of the low S/N star (with blue color) and TINYTIM PSFs is a bit worse in the same radius range (compared to the high S/N PSF).

In Figures 7–16 we present the UCD color profiles, obtained with the TINYTIM PSF (with the average UCD color and of a very large size) and the low S/N star, but due to the above reasons we prefer to trust the TINYTIM PSF more.

Having done all of this, we conclude that the color gradient is most reliable in the region $\sim$4–54 pixels ($\sim$7.5–100 pc for Virgo and $\sim$9–124 pc for Fornax). The uncertainties in the PSF structure become significant outside this radius range. In addition to the PSF effects, we cannot trust the color gradient beyond $R \sim$ 60–80 pc for most of the UCDs due to the noticeable deviation between the GALFIT model and the data. The color gradient may be incorrectly amplified because of it. To highlight the region where we consider the color gradient is reliable (the *"trusted region"*), we draw two vertical lines in all the panels: at the outer radius where object-minus-model residuals start to deviate from zero significantly, and at the inner radius where there may be uncertainties in the structure of the

[13] See http://www.stsci.edu/software/tinytim.

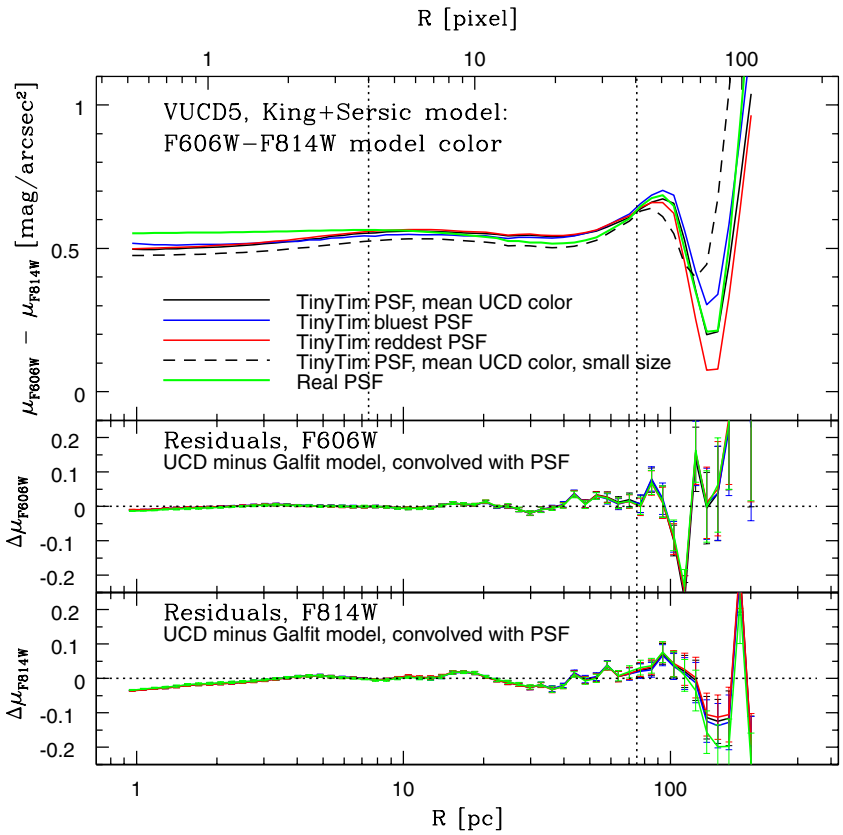

Figure 8. VUCD5 color profile.

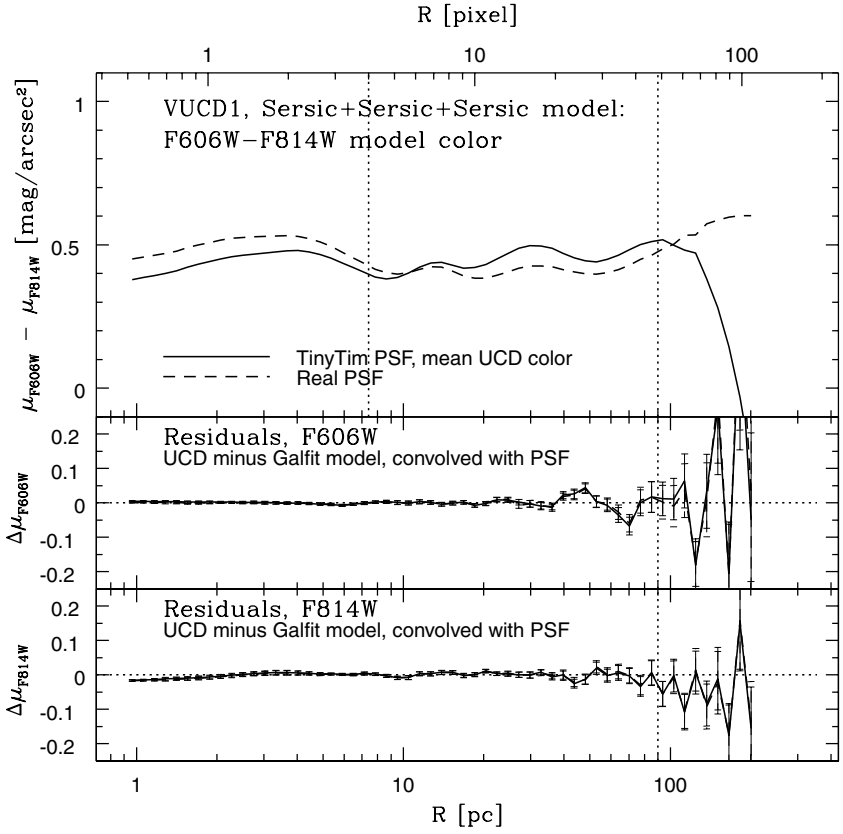

Figure 9. VUCD1 color profile.

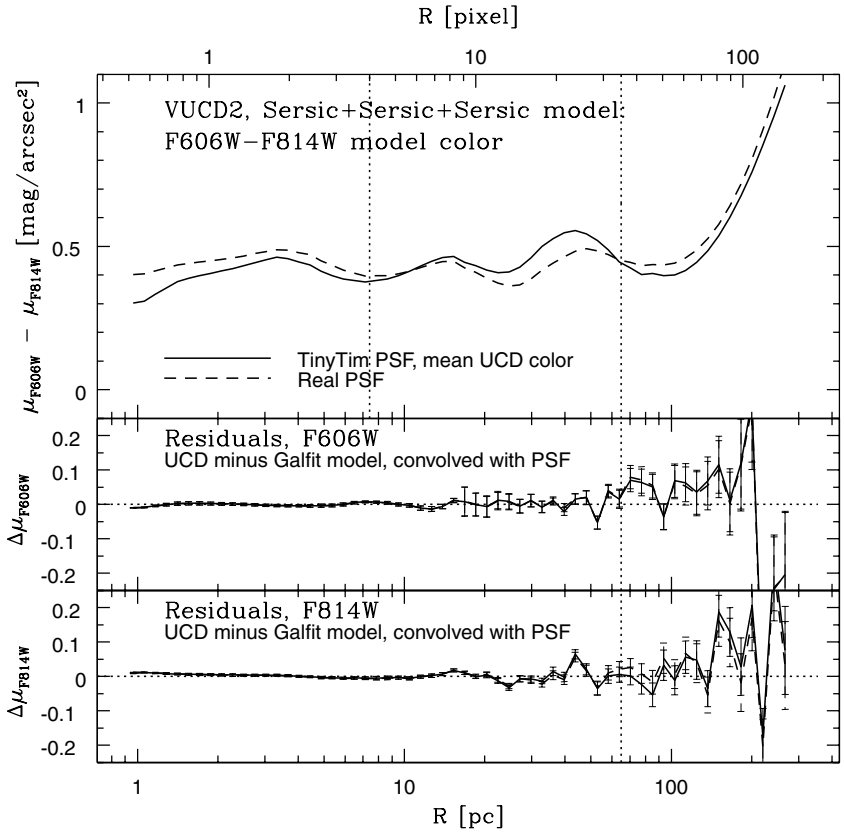

Figure 10. VUCD2 color profile.

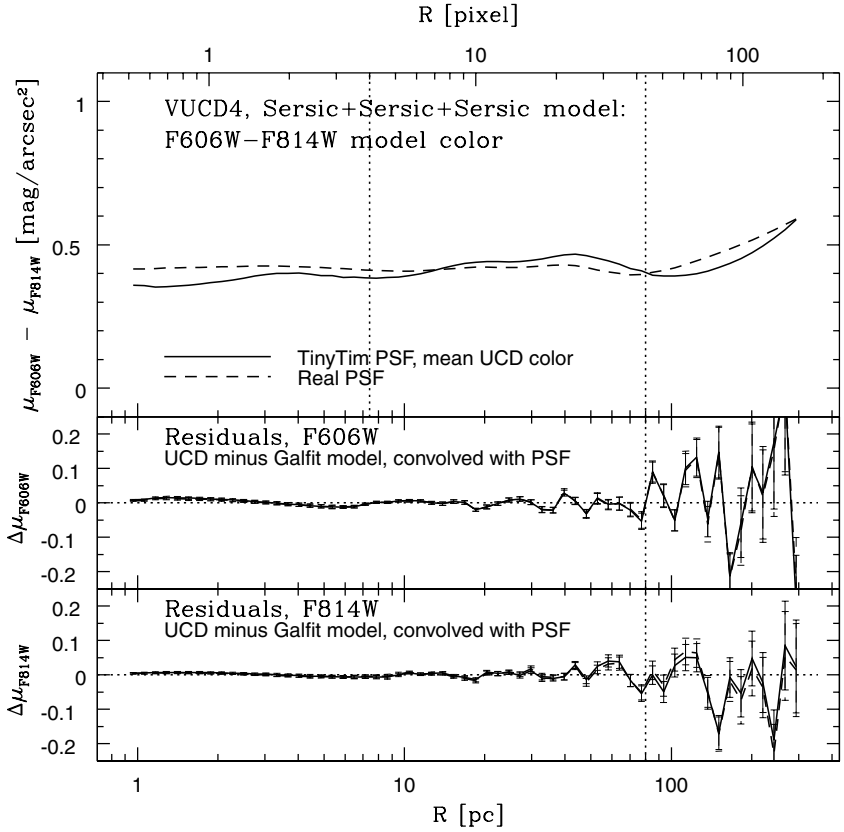

Figure 11. VUCD4 color profile.

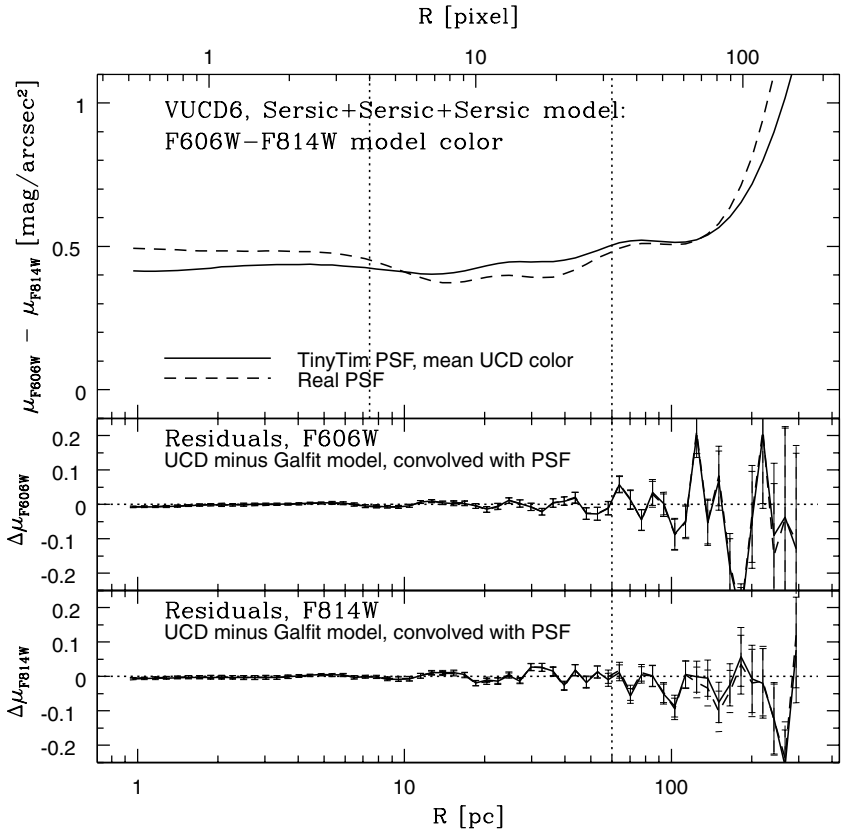

Figure 12. VUCD6 color profile.

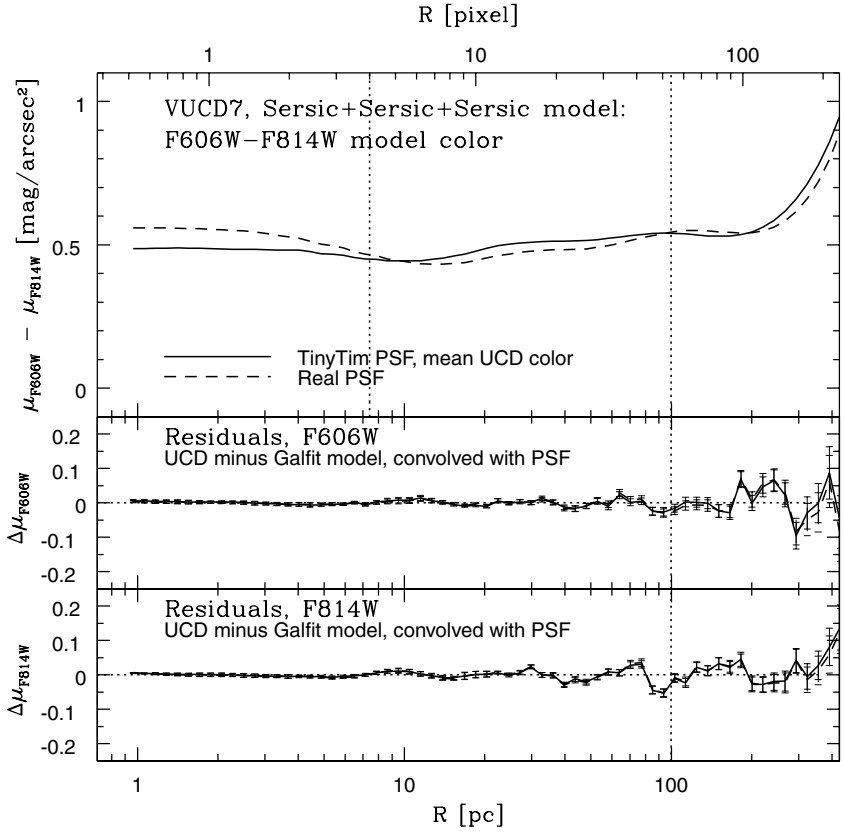

Figure 13. VUCD7 color profile.

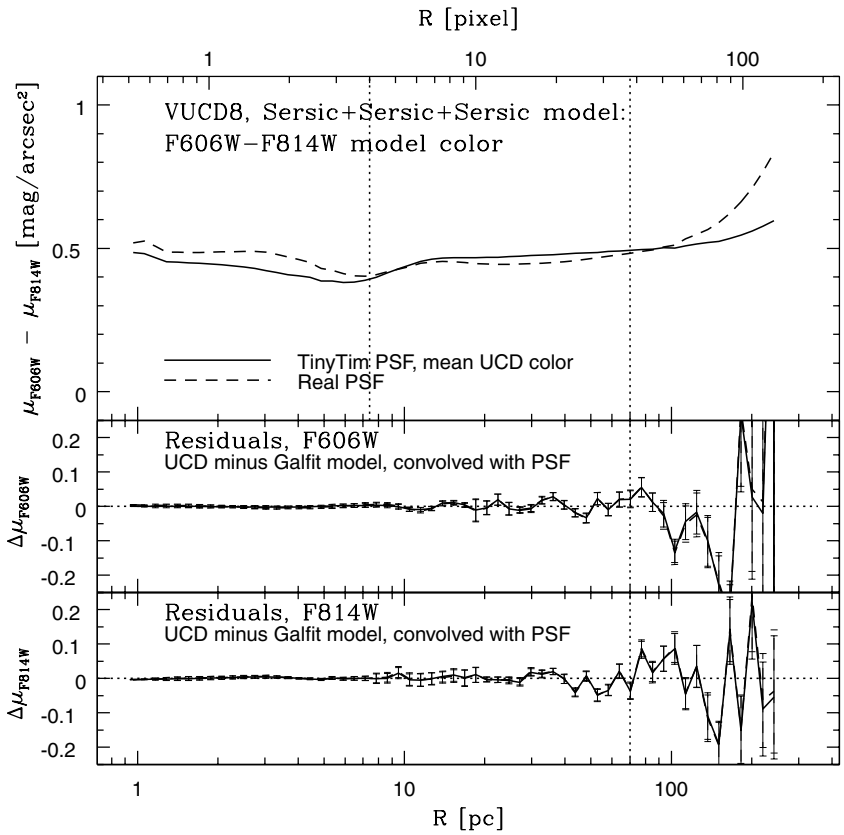

Figure 14. VUCD8 color profile.

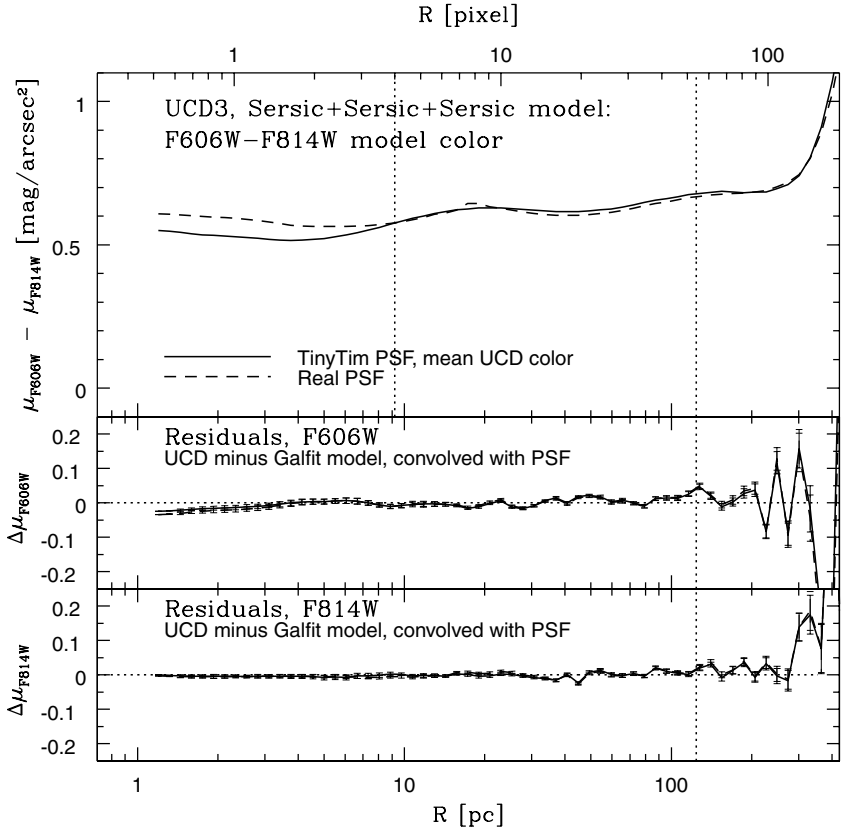

Figure 15. UCD3 color profile.

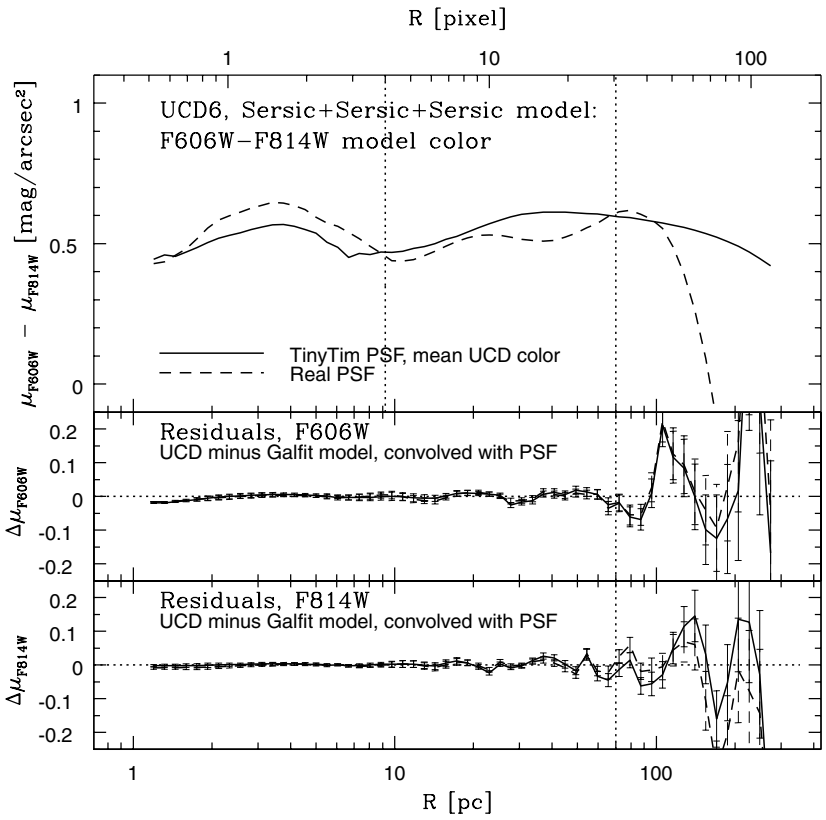

Figure 16. UCD6 color profile.

PSF core. For VUCD3, for example, the "trusted region" is ∼7.5–75 pc (Figure 7).

3. Sky subtraction. The sky (background) was initially subtracted from the UCD images by MULTIDRIZZLE. We then applied additional background corrections, determined from empty parts of the images. Finally, we fitted the background when fitting UCDs with GALFIT. For the latter, we did the fitting over very large area, masking out the HRC "occulting finger" and all the background/foreground objects in the image, except objects appearing very close to the UCDs. We fitted and subtracted such objects from the image, which is more accurate than masking. Note that besides the mean sky level, GALFIT finds the gradient in the sky. The sky level is determined very well, as seen from the absence of a trend in the residuals in Figures 7–16 (except for VUCD2).

The results of the color profile fitting are shown in Figures 7–16. The main observational conclusion is that, with two exceptions, all the UCDs appear to have small positive color gradients in the sense of getting redder outward: mean $\Delta(\mathrm{F606W} - \mathrm{F814W}) = 0.14$ mag per 100 pc with rms $= 0.06$ mag per 100 pc. The two exceptions are VUCD2 and UCD3. It is hard to make very strong conclusions regarding VUCD2 because of the large fluctuations in the color profile and a slight systematic trend (upward) in the residuals. We would also consider the UCD3 color gradient as unreliable, since we did not model and subtract the background spiral (see Section 3 and Evstigneeva et al. 2007b). It is very hard to separate this faint object from the UCD reliably. We did all the modeling for the half of the UCD, which is less affected by the spiral, but we cannot prove that it is completely unaffected. There still can be some flux from this spiral, projected onto the UCD3 center and making it slightly bluer.

4.3.2. Interpretation

We stress that this discussion only applies to the brightest UCDs for which it was possible to estimate the color gradients.

First we consider the hypothesis that UCDs are very luminous GCs.

Djorgovski et al. (1991) report color gradients in MW GCs. They find that the clusters with post core collapse morphology (with central cusps) have positive color gradients (in the same sense as the gradient in the UCDs), while clusters with King model morphology (with flat cores) do not show any color gradient. Djorgovski et al. interpret this as evidence that the dynamical evolution of clusters can modify their stellar populations. Core collapse tends to affect more massive stars, with lower mass stars (red sub dwarfs) tending to move to larger average radii. The Djorgovski et al. study may not, however, be relevant to UCDs. Their measurements only extend to 1–8 pc from the cluster center and, more importantly, relaxation and mass segregation (less massive red sub dwarfs sitting outside) would not work for systems as large as UCDs. Their half-mass relaxation times are ∼8 Hubble times (for the Virgo UCDs with the dynamical and structural parameters from Evstigneeva et al. 2007b) and larger than a Hubble time for radii $R > 8$ pc where we have our color gradient measurements. There has not been sufficient time to drive the low mass stars toward large radii. Also, in a later work, Sohn et al. (1996) found positive color gradients in GCs with King model morphology (they went to a larger radius from the center, 11–19 pc), and made a conclusion that the color gradient is not unique to post core collapse GCs and, hence, may not be explained by the dynamical evolution. Still more recently, Sohn et al. (1998) found both negative and positive color gradients in GCs with both post core collapse and King model morphology.

Other possible interpretations of the UCD color gradients could be that UCDs were born mass-segregated (primordial mass segregation, if it has not been erased because the relaxation times are long); or that UCDs are composed of multiple (at least two) stellar populations. It is actually unlikely we are seeing mass segregation as most of the light from these old populations is mainly coming from upper main-sequence stars and giants with a relatively small mass range. On the other hand, some of the brightest MW GCs (e.g., ω Cen, NGC 2808, and NGC 1851) are found to contain multiple stellar populations (e.g., Milone et al. 2008). ω Cen is the only GC for which we have information about the radial distribution of stellar populations (Hilker & Richtler 2000; Sollima et al. 2007). Hilker & Richtler (2000) studied the two major populations (of RGB stars) in ω Cen (it has at least three sub-populations) and found that the younger, more metal-rich population is more centrally concentrated than the older, more metal-poor population. This gives a negative color gradient—opposite to what we find for UCDs. A possible explanation for ω Cen is that a more centrally concentrated population formed at a later time from enriched material. Assuming the same scenario for UCDs, we can test if it agrees with the UCD color gradients. For Virgo UCD ages (8–15 Gyr), metallicities ([Z/H] $= -1.35$ to -0.17 dex), and colors ($V-I = 0.96$–1.13 mag) (Evstigneeva et al. 2007b), and using Maraston (2005) SSP models, we consider the following model populations: a more metal rich ([Z/H] $= -0.33$ dex), younger (8 Gyr) population with $V-I = 1.08$ mag, and a more metal poor ([Z/H] $= -1.35$ dex), older (15 Gyr) population with $V-I = 0.98$ mag. The colors are obtained for a Salpeter IMF (the Kroupa IMF gives very similar results). The sum of these two populations will give total ages, metallicities, and colors similar to those observed in the UCDs. The color gradient, however, is negative—opposite to what is observed in the UCDs (although the same as in ω Cen). This suggests that the star-formation histories in UCDs and ω Cen are different, but this still does not prove that UCDs are different to GCs. Recent work by Milone et al. (2008), for example, says that three different GCs with multiple stellar populations (ω Cen, NGC 2808, and NGC 1851) all have different star-formation histories. Milone et al. also note that "the star-formation history of a GC can vary strongly from cluster to cluster" and they point out that the multiple stellar populations have only been detected in the most massive MW GCs. They suggest that "cluster mass might have a relevant role in the star-formation history of GCs."

From these results we conclude that UCDs may contain multiple stellar populations without contradicting the hypothesis that they are bright GCs. However, a lot more has to be done in terms of both observational work and theory/simulations (as was concluded by D'Antona & Caloi 2007) to understand the origin of multiple stellar populations in UCDs and GCs. Obviously, something happens in very massive/luminous GCs so that they have multiple stellar populations. It might be that their gravitational potential is strong enough to keep the gas that would otherwise be completely expelled by stellar winds and supernovae explosions (see, e.g., Baumgardt et al. 2008) and that the second (and other) generations of stars formed from this gas.

We now consider the alternative hypothesis that UCDs are the nuclei of threshed galaxies.

It could be argued that the color gradients in UCDs are consistent with the threshing hypothesis for the formation of UCDs from dE,Ns. Lotz et al. (2004) showed for Fornax cluster dE,Ns, using aperture photometry, that their stellar envelopes are 0.1–0.2 mag redder in $V-I$ than their nuclei. In this case, residual stars from the envelope after the disruption process would naturally explain the color gradient in UCDs. We can test this with more recent data from the ACS Virgo Cluster Survey for early-type galaxies. We compared the colors of the nuclei (Côté et al. 2006) and their underlying galaxies (Ferrarese et al. 2006): the nuclei are bluer than their underlying galaxies for dEs ($M_B > -17.6$ mag), which is consistent with the Lotz et al. findings, while for giant Es ($M_B < -17.6$ mag) the nuclei are redder than their underlying galaxies. These results are in agreement with the color gradients found in dwarf and giant elliptical galaxies. Dwarf elliptical galaxies have mostly positive color gradients (getting redder outward, e.g., Vader et al. 1988), while luminous early-type galaxies have generally negative color gradients (getting bluer outward, e.g., de Propris et al. 2005a). Vader et al. (1988) explain the origin of positive color gradients in early-type dwarf galaxies by age gradients, as metallicity gradients are removed by galactic winds. Brighter galaxies have a deeper potential well. For them, galactic winds will be important in the outer parts only. This is why bright galaxies have stronger metallicity gradients.

If UCDs are formed by *simple* stripping of dEs (with no other processes involved, like effects of gas removal on the chemical evolution of nuclei), the UCD color gradients are in agreement with the threshing hypothesis (with both dE color gradients and dE core/envelope colors). There is a problem with the brightest and reddest UCDs, however. If we have a look at the CMDs (Figures 4 and 5), VUCD3, VUCD7, and UCD3 are all located in the region where only giant elliptical galaxy nuclei are found. If we interpret the fact that VUCD7 and UCD3 have envelopes as incomplete stripping and consider only the cores of these UCDs in the CMDs, the cores will then be in the same region as dE nuclei. (The cores of all the UCDs with envelopes have magnitudes and colors as follows: $-11.16 \geqslant M_V \geqslant -12.39$ mag, $0.92 \leqslant V-I \leqslant 1.18$ mag.) Thus, VUCD7 and UCD3 may still be threshed dE galaxies. VUCD3 does not have an envelope but it is very bright and very red, so it does look like a giant elliptical galaxy nucleus. However, VUCD3 has a positive color gradient which we might not expect in a giant elliptical galaxy. It may be possible to argue that VUCD3 is a threshed late-type galaxy (if we still prefer the threshing hypothesis), since late-type galaxies have mostly positive color gradients (e.g., Taylor et al. 2005).

It may also be possible that UCDs are genuine, but anomalous, dwarf galaxies (requiring no threshing). Their positive color gradients are consistent with dE galaxy color gradients—the pure age gradients, explained by galactic winds (as above). If we assume that UCDs have younger stellar populations in the center (7 Gyr) and older populations in the outer regions (15 Gyr), then for a metallicity of [Z/H] $= -0.33$ dex (same for the two populations), Maraston (2005) SSP models with a Salpeter IMF will give us the color variation from $V-I = 1.06$ mag in the center to $V-I = 1.16$ mag outside; or for a metallicity of [Z/H] $= -1.35$ dex: from $V-I = 0.90$ mag in the center to $V-I = 0.99$ mag outside. This is consistent with what we see in the UCDs.

Our conclusion is that the positive color gradients found in bright UCDs (two Fornax UCDs and eight Virgo UCDs) are consistent with them being either bright GCs or threshed dE galaxies (except for VUCD3). However, the spectroscopic ages, metallicities, and α-abundances for Virgo UCDs, obtained in our previous work (Evstigneeva et al. 2007b), are not consistent with the formation of UCDs by the simple removal of the envelope

from the nuclei of dE galaxies. Since spectroscopic ages and metallicities are more powerful tools than colors (colors are degenerate), we have to reject the threshing hypothesis for the Virgo UCD origin. Hence, the Virgo UCDs are more consistent with being bright GCs. As for the two Fornax UCDs, no firm conclusions on their origins can be drawn without having spectroscopic age, metallicity, and α-abundance estimates for them. At the moment, we can only say that their color gradients are consistent with all three hypotheses: threshed dE galaxies, bright GCs, and genuine dwarf galaxies.

5. SUMMARY

In this paper, we have presented analysis of the structure and colors of the most extensive and complete sample of UCDs in the Fornax and Virgo Clusters observed to date: thirteen Fornax UCDs with magnitudes in the range $-10.49 \geqslant M_V \geqslant -13.33$ mag and eight Virgo UCDs with magnitudes $-11.95 \geqslant M_V \geqslant -13.42$ mag. The sample includes six Virgo UCDs initially presented by Evstigneeva et al. (2007b), as we have made several improvements to the image analysis. The main results of our analysis are as follows.

1. We have modeled the images of Fornax and Virgo UCDs using the two-dimensional fitting algorithm GALFIT, assuming empirical King, Sérsic, and Nuker models (or King+Sérsic and Sérsic+Sérsic) for the luminosity profile. We find that for the faint UCDs ($m_{V,0} \sim$ 19.9–20.9 mag), there is no preference of one model over another: all the models (Nuker, King, and Sérsic) fit the UCDs equally well. The bright UCDs ($m_{V,0} \sim$ 17.5–18.9 mag) have extended outer halos best fitted by two-component models (King+Sérsic or Sérsic+Sérsic) or a double power law (Nuker). This does not mean that bright and faint UCDs are intrinsically different. With deeper observations for the fainter UCDs, we could possibly detect outer halos in them were any present. The detection of these extended halos around luminous UCDs is not consistent with their having the standard King profiles traditionally associated with GCs, but recent work of McLaughlin & van der Marel (2005) and McLaughlin et al. (2008) has shown that extended halos are a general characteristic of massive GCs in the MW and some of its satellites and NGC 5128.
   Our modeling also shows that the UCDs have a range of Sérsic indices n and King concentrations c, as well as a range of central slopes (seen from Nuker inner slopes γ): from flat "King" cores to central cusps. This suggests that convolving some cuspy models with the PSF allows such models to fit the seeing-blurred centers of some UCD profiles. We, however, cannot make very strong conclusions regarding central cusps or cores in the UCDs, taking into account the resolution and other limits of our data.
   We do not find any correlations between the model parameters mentioned above and the UCD luminosity, size, or color. Furthermore, no correlation of ellipticity with luminosity, size, or color has been found for the UCDs.
   The two-sample K-S and Wilcoxon tests show that the UCD ellipticities are consistent with extragalactic GC distributions (NGC 5128 and M31 GCs), but significantly different from the MW GC distribution.
2. We have shown that UCDs and GCs form a continuous distribution across the luminosity–size plane, but UCDs seem to be different to *typical* GCs in the sense that the UCDs have sizes correlated with luminosities whereas the GCs do not. We obtain the following luminosity–size relation for the UCDs in our sample: $R_{\rm eff} \propto L_V^{0.88\pm0.13}$ or $R_{\rm eff} \propto L_V^{0.68\pm0.13}$ (if we exclude two brightest objects). However, the luminosity–size relation we observe for the UCDs is similar to observations for most *luminous* GCs: Barmby et al. (2007) report an increasing lower bound on $R_{\rm eff}$ in the mass versus $R_{\rm eff}$ plane for the most massive GCs. The nuclei of early-type galaxies (from Côté et al. 2006) with luminosities similar to the UCDs show a luminosity–size correlation with the same slope as the UCD relation, but we find that the effective radii of the UCDs are systematically ~ 2.2 times larger than the nuclei of the same luminosity. This difference is significant at a confidence level $> 99.9\%$.
   Although this observation is superficially inconsistent with a process whereby these galaxy nuclei are stripped to form UCDs, the change in size may be a result of the stripping process. The simulations of the stripping process by Bekki et al. (2001, 2003) indicate some expansion of the remnant core, but no quantitative results are provided. Given our new observational result, it will be important to test this in detail against simulations of the threshing process to see if it is consistent with the size difference we have found between UCDs and the early-type galaxy nuclei.
   We also note that the nuclei of late-type galaxies are similar to the nuclei of early-type galaxies (and UCDs) in terms of luminosities and sizes. This means that UCDs—if formed by disruption—could be the remnant nuclei of both early-type and late-type galaxies, not just dE,Ns as was initially suggested.
3. The UCD total magnitudes and colors (their position in the CMDs) are consistent with them being either luminous GCs or threshed nuclei of both early-type and late-type galaxies.
4. We have estimated radial color gradients for the brightest UCDs in our sample: Virgo UCDs and Fornax UCD3 and UCD6. All the UCDs (with two exceptions) appear to have small positive color gradients in the sense of getting redder outward: mean Δ(F606W$-$F814W) $= 0.14$ mag per 100 pc with rms $= 0.06$ mag per 100 pc. The two exceptions are VUCD2 and UCD3: the color gradient estimates for them are unreliable.
   The positive color gradients found in the bright UCDs are consistent with them being either bright GCs or threshed dE galaxies (except VUCD3). However, the spectroscopic ages, metallicities, and α-abundances for Virgo UCDs, obtained in our previous work (Evstigneeva et al. 2007b), are not consistent with the formation of UCDs by the *simple* removal of the envelope from the nuclei of dE galaxies. Since spectroscopic ages and metallicities are more powerful tools than colors, we have to reject the threshing hypothesis for the Virgo UCD origin. Hence, the Virgo UCDs are more consistent with being bright GCs. As for the two Fornax UCDs, no firm conclusions on their origins can be drawn without having spectroscopic age, metallicity, and α-abundance estimates for them. At the moment, we can only say that their color gradients are consistent with them being threshed dE galaxies, bright GCs, and genuine dwarf galaxies.

The aim of our investigation was to test two formation hypotheses for UCDs—whether they are bright GCs or threshed early-type dwarf galaxies—by direct comparison of UCD structural parameters and colors with GCs and galaxy nuclei. In most

of the measurements we have made (profiles, color–magnitude relations, color gradients), the UCDs display properties consistent with a threshing origin and with what might be expected for luminous GCs. We therefore conclude that these structural parameters and colors are not able to distinguish sufficiently between the different formation hypotheses.

The one exception to this conclusion is the difference we find in the size–luminosity relation between UCDs and the nuclei of early-type galaxies. This significant difference (the UCDs are 2.2 times as large as nuclei at the same luminosity) suggests an important numerical test of the threshing hypothesis: it should be relatively easy to predict the increase in the size of nuclei resulting from the threshing hypothesis and compare that to our new observational results.

This work has been supported by a Discovery Project grant from the Australian Research Council. Part of the work reported here was done at the Institute of Geophysics and Planetary Physics, under the auspices of the U.S. Department of Energy by Lawrence Livermore National Laboratory in part under contract W-7405-Eng-48 and in part under contract DE-AC52-07NA27344. The authors wish to thank Harry Ferguson (STScI) and Anton Koekemoer (STScI) for their assistance with the *HST* data analysis, Holger Baumgardt (University of Bonn) for helpful discussions and the referee for their very careful reading of our paper and many helpful suggestions.

Facilities: HST (ACS)

REFERENCES

Barmby, P., McLaughlin, D. E., Harris, W. E., Harris, G. L. H., & Forbes, D. A. 2007, AJ, 133, 2764
Baumgardt, H., Kroupa, P., & Parmentier, G. 2008, MNRAS, 384, 1231
Bekki, K., Couch, W. J., & Drinkwater, M. J. 2001, ApJ, 552, L105
Bekki, K., Couch, W. J., Drinkwater, M. J., & Shioya, Y. 2003, MNRAS, 344, 399
Böker, T., Laine, S., van der Marel, R. P., Sarzi, M., Rix, H.-W., Ho, L. C., & Shields, J. C. 2002, AJ, 123, 1389
Böker, T., Sarzi, M., McLaughlin, D. E., van der Marel, R. P., Rix, H.-W., Ho, L. C., & Shields, J. C. 2004, AJ, 127, 105
Burstein, D., Bender, R., Faber, S., & Nolthenius, R. 1997, AJ, 114, 1365
Bruzual, G., & Charlot, S. 2003, MNRAS, 344, 1000
Côté, P., et al. 2004, ApJS, 153, 223
D'Antona, F., & Caloi, V. 2007, in Proc. of IAU Symp. 246, Dynamical Evolution of Dense Stellar Systems, ed. E. Vesperini, M. Gierzs, & A. Sills (Dordrecht: Kluwer), 156
Côté, P., et al. 2006, ApJS, 165, 57
De Propris, R., Colless, M., Driver, S. P., Pracy, M. B., & Couch, W. 2005a, MNRAS, 357, 590
De Propris, R., Phillipps, S., Drinkwater, M. J., Gregg, M. D., Jones, J. B., Evstigneeva, E., & Bekki, K. 2005b, ApJ, 623, L105
Djorgovski, S., Piotto, G., Phinney, E. S., & Chernoff, D. F. 1991, ApJ, 372, L41
Drinkwater, M. J., Gregg, M. D., Couch, W. J., Ferguson, H. C., Hilker, M., Jones, J. B., Karick, A., & Phillipps, S. 2004, Publ. Astron. Soc. Aust., 21, 375
Drinkwater, M. J., Gregg, M. D., Hilker, M., Bekki, K., Couch, W. J., Ferguson, H. C., Jones, J. B., & Phillipps, S. 2003, Nature, 423, 519
Drinkwater, M. J., Jones, J. B., Gregg, M. D., & Phillipps, S. 2000a, PASA, 17, 227
Drinkwater, M. J., et al. 2000b, A&A, 355, 900
Elson, R. A. W. 1999, in Globular Clusters, Cambridge Contemporary Astrophysics, ed. C. Martínez Roger, I. Pérez Fournon, & F. Sánchez (Cambridge: Cambridge Univ. Press)
Evstigneeva, E. A., Drinkwater, M. J., Jurek, R., Firth, P., Jones, J. B., Gregg, M. D., & Phillipps, S. 2007a, MNRAS, 378, 1036
Evstigneeva, E. A., Gregg, M. D., Drinkwater, M. J., & Hilker, M. 2007b, AJ, 133, 1722
Fellhauer, M., & Kroupa, P. 2002, MNRAS, 330, 642
Ferrarese, L., et al. 2006, ApJS, 164, 334
Freedman, W. L., et al. 2001, ApJ, 553, 47
Graham, A. W., Erwin, P., Trujillo, I., & Ramos, A. A. 2003, AJ, 125, 2951
Gregg, M. D., et al. 2008, AJ, submitted
Harris, W. E. 1996, AJ, 112, 1487
Harris, W. E., Harris, G. L. H., Holland, S. T., & McLaughlin, D. E. 2002, AJ, 124, 1435
Haşegan, M., et al. 2005, ApJ, 627, 203
Hilker, M., Baumgardt, H., Infante, L., Drinkwater, M., Evstigneeva, E., & Gregg, M. 2007, A&A, 463, 119
Hilker, M., Infante, L., Vieira, G., Kissler-Patig, M., & Richtler, T. 1999, A&AS, 134, 75
Hilker, M., & Richtler, T. 2000, A&A, 362, 895
Holland, S., Coté, P., & Hesser, J. E. 1999, A&A, 348, 418
Jones, J. B., et al. 2006, AJ, 131, 312
Jordán, A., et al. 2007, ApJS, 169, 213
Karick, A., Gregg, M.D., & Drinkwater, M. J. 2008, AJ, submitted
Larsen, S. S., Brodie, J. P., Huchra, J. P., Forbes, D. A., & Grillmair, C. J. 2001, AJ, 121, 2974
Lauer, T. R., Ajhar, E. A., Byun, Y.-I., Dressler, A., Faber, S. M., Grillmair, C., Kormendy, J., Richstone, D., & Tremaine, S. 1995, AJ, 110, 2622
Liske, J., Driver, S. P., Allen, P. D., Cross, N. J. G., & De Propris, R. 2006, MNRAS, 369, 1574
Lotz, J. M., Miller, B. W., & Ferguson, H. C. 2004, ApJ, 613, 262
Maraston, C. 2005, MNRAS, 362, 799
McLaughlin, D. E., Barmby, P., Harris, W. E., Forbes, D. A., & Harris, G. L. H. 2008, MNRAS, 384, 563
McLaughlin, D. E., & van der Marel, R. P. 2005, ApJS, 161, 304
Mieske, S., Hilker, M., & Infante, L. 2002, A&A, 383, 823
Mieske, S., Hilker, M., Infante, L., & Jordán, A. 2006, AJ, 131, 2442
Mieske, S., Hilker, M., Jordán, A., Infante, L., & Kissler-Patig, M. 2007, A&A, 472, 111
Mieske, S., et al. 2004, AJ, 128, 1529
Milone, A. P., et al. 2008, ApJ, 673, 241
Peng, C. Y., Ho, L. C., Impey, C. D., & Rix, H.-W. 2002, AJ, 124, 266
Peng, E. W., et al. 2006, ApJ, 639, 95
Rossa, J., van der Marel, R. P., Böker, T., Gerssen, J., Ho, L. C., Rix, H.-W., Shields, J. C., & Walcher, C.-J. 2006, AJ, 132, 1074
Schlegel, D. J., Finkbeiner, D. P., & Davis, M. 1998, ApJ, 500, 525
Sérsic, J. L. 1968, Atlas de Galaxias Australes (Córdoba: Obs. Astron., Univ. Nac. Córdoba)
Sirianni, M., et al. 2005, PASP, 117, 1049
Sohn, Y.-J., Byun, Y. I., & Chun, M.-S. 1996, Ap&SS, 243, 379
Sohn, Y.-J., Byun, Y. I., Yim, H.-S., Rhee, M.-H., & Chun, M.-S. 1998, JASS, 15, 1
Sollima, A., Ferraro, F. R., Bellazzini, M., Origlia, L., Straniero, O., & Pancino, E. 2007, ApJ, 654, 915
Taylor, V. A., Jansen, R. A., Windhorst, R. A., Odewahn, S. C., & Hibbard, J. E. 2005, ApJ, 630, 784
Vader, J. P., Vigroux, L., Lachièze-Rey, M., & Souviron, J. 1988, A&A, 203, 217
Walcher, C.-J., Böker, T., Charlot, S., Ho, L. C., Rix, H.-W., Rossa, J., Shields, J. C., & van der Marel, R. P. 2006, ApJ, 649, 692
Walcher, C.-J., et al. 2005, ApJ, 618, 237
Wehner, E., & Harris, W. 2007, ApJ, 668, L35